

BOSTON UNIVERSITY
COLLEGE OF ENGINEERING

Thesis

**MICRO SCALE OSCILLATING HEAT PIPES
FOR ELECTRONICS COOLING**

by

MICHAEL SHOHET

B.A., University of Massachusetts Amherst, 2020
B.A., University of Massachusetts Amherst, 2020

Submitted in partial fulfillment of the
requirements for the degree of

Master of Science

2025

© 2025 by
MICHAEL SHOHET
All rights reserved

Approved by

First Reader

Chuanhua Duan, Ph.D.
Associate Professor of Mechanical Engineering
Associate Professor of Materials Science and Engineering

Second Reader

Kamil L. Ekinci, Ph.D.
Professor of Mechanical Engineering
Professor of Materials Science and Engineering

Third Reader

Raymond Nagem, Ph.D.
Associate Professor of Mechanical Engineering

MICRO SCALE OSCILLATING HEAT PIPES
FOR ELECTRONICS COOLING
MICHAEL SHOHET

ABSTRACT

Effective thermal management is critical to the reliable operation and longevity of modern semiconductor devices. As transistor densities continue to increase with each successive generation of chips, power consumption rises, leading to escalating heat fluxes. Conventional cooling methods, such as air-cooled heat sinks or liquid cooling loops, are highly effective at dissipating heat. However, as devices continue to shrink, the need arises for thermal management solutions capable of efficiently transporting heat from densely packed electronic components to remote heat sinks to aid in heat dissipation. Consequently, the miniaturization of thermal management technologies has become increasingly important, enabling the development of solutions that can be seamlessly integrated with densely packed semiconductor devices to facilitate efficient heat transport and maintain performance at smaller scales.

Oscillating heat pipes (OHPs) have emerged as a promising candidate for high-performance thermal management due to their passive operation, high thermal conductivity, and capacity to handle large heat fluxes. Miniaturizing OHPs to the microscale offers the potential to improve heat dissipation in semiconductor devices by enabling efficient heat transport over extended lengths, despite having micro-scale cross-sections. This capability is particularly advantageous for extracting heat from compact electronic systems and delivering it to remote cooling units. However, achieving reliable

performance in micro-scale oscillating heat pipes (MOHPs) presents unique challenges related to fluid behavior, capillary limits, and dry-out conditions.

This work investigates several design enhancements aimed at improving the performance and operational stability of MOHPs. Three specific approaches are examined: (1) the implementation of alternating hydraulic diameters to promote improved fluid circulation compared to uniform channels; (2) the integration of reentrant mushroom-shaped structures designed to mitigate liquid flooding and serve as persistent nucleation sites for vapor formation; and (3) the incorporation of micro-grooved wick structures within the channels to increase capillary flow capacity and delay the onset of dry-out. These design modifications aim to address key limitations in micro-scale OHPs and enhance their viability as a next-generation cooling solution for high-power semiconductor devices.

TABLE OF CONTENTS

Abstract	iv
Table of Contents	vi
List of Tables	viii
List of Figures	ix
List of Abbreviations	x
1. Introduction	1
2. Background	4
3. Device Design	12
a. Mushroom Shaped Reentrant Structures	12
b. Micro-Grooved Wick Structures	15
c. Dual Diameter vs. Single Diameter Channels	16
d. Design Cases	17
4. Fabrication	20
5. Experimental Design	22
a. Device Filling	22
i. Filling Setup 1	23
ii. Filling Setup 2	25
iii. Filling Setup 3	27
iv. Filling Setup 4	28
b. Experimental Setup	29
c. Methodology	32

6. Results	34
7. Conclusions & Continuing Work	48
Bibliography	52
VITA	55

LIST OF TABLES

Table 1: Heat entering Devices	37
Table 2: Energy Efficiency	38

LIST OF FIGURES

1. Schematic of an Oscillating Heat Pipe	2
2. Operation of Reentrant Structures	7
3. Flow Boiling With & Without Capillary Structures	9
4. Different Types of Cavities Illustrating Resilience Against Flooding	13
5. Schematic of Double & Single Diameter Channels	17
6. Overview of Device Designs	20
7. Overview of Device Fabrication	22
8. Schematic of Filling Setup 1	23
9. Consequences of Filling Setup 2	26
10. Schematic of Filling Setup 3	28
11. Schematic of Filling Setup 4	29
12. Schematic of the Experimental Setup	30
13. Rendering of the Evaporator and Condenser	31
14. Simulation of Heat Transfer through Copper Block & Experimental Data	36
15. Power Efficiency of all Tested Devices	38
16. Power Efficiency of Single Diameter and Dual Diameter Baseline Cases	40
17. Power Efficiency of all Single Diameter Devices	41
18. Dryout Comparison of Single Diameter Wick and Dual Diameter	42
19. Dryout Comparison of Single and Dual Diameter Wick Devices	44
20. Power Efficiency of Single and Dual Diameter Wick Devices	44
21. Power Efficiency of all Dual Diameter Devices	46

LIST OF ABBREVIATIONS

CPU	...	Central Processing Unit
DRIE	...	Deep Reactive Ion Etching
HF	...	Hydrofluoric Acid
HVAC	...	Heating, Ventilation, Air Conditioning
MOHP	...	Micro Oscillating Heat Pipe
OHP	...	Oscillating Heat Pipe
PDMS	...	Polydimethylsiloxane
RIE	...	Reactive Ion Etching
TMAH	...	Tetramethylammonium Hydroxide
UV	...	Ultraviolet

1. Introduction

Rapid advancements in semiconductor device technologies have led to increasing transistor densities and power consumption in modern electronics. As devices become more compact and more powerful, thermal management has become critical to ensuring reliable high performance in such devices. Excess heat can lead to degraded performance, device destruction, and system failures [1,2]. Replacing individual devices and systems is becoming increasingly expensive as these technologies become more complex. As such, it is highly desirable to be able to mitigate the effects of extreme heat.

Traditional cooling methods, such as heat sinks and water loops have proven to be effective solutions. However, as device architecture becomes increasingly dense, and heat fluxes continue to escalate, there is growing interest in alternative thermal management techniques that are capable of transporting heat away from devices, and in particular, from specific areas of devices that act as localized hot spots. This, in turn, has driven research into novel heat transfer technologies capable of functioning at small scales.

One promising approach is the oscillating heat pipe [3,4]. A derivation of traditional heat pipes, the oscillating heat pipe (OHP) is a device that is typically structured as a serpentine loop of channels. Device operation begins with the device partially filled with fluid in the liquid state. An external heat source applies a heat flux to one side of the OHP, which serves to cause bubble nucleation. Bubbles containing vapor, referred to as vapor plugs, expand as heat continues to be applied. This expansion drives the remaining liquid, which forms liquid slugs in between bubbles, to the other side of the device, where an external condenser acts as a heat sink. Energy is removed from the

fluid, and as this occurs, vapor condenses back into the liquid state. Condensation causes contraction or collapse of vapor plugs, generating pressure differences that drive the liquid back to the evaporator side, where the cycle repeats. In this way, oscillatory motion occurs, operated passively and driven purely by phase change phenomena. A schematic of this device is shown in figure 1 below.

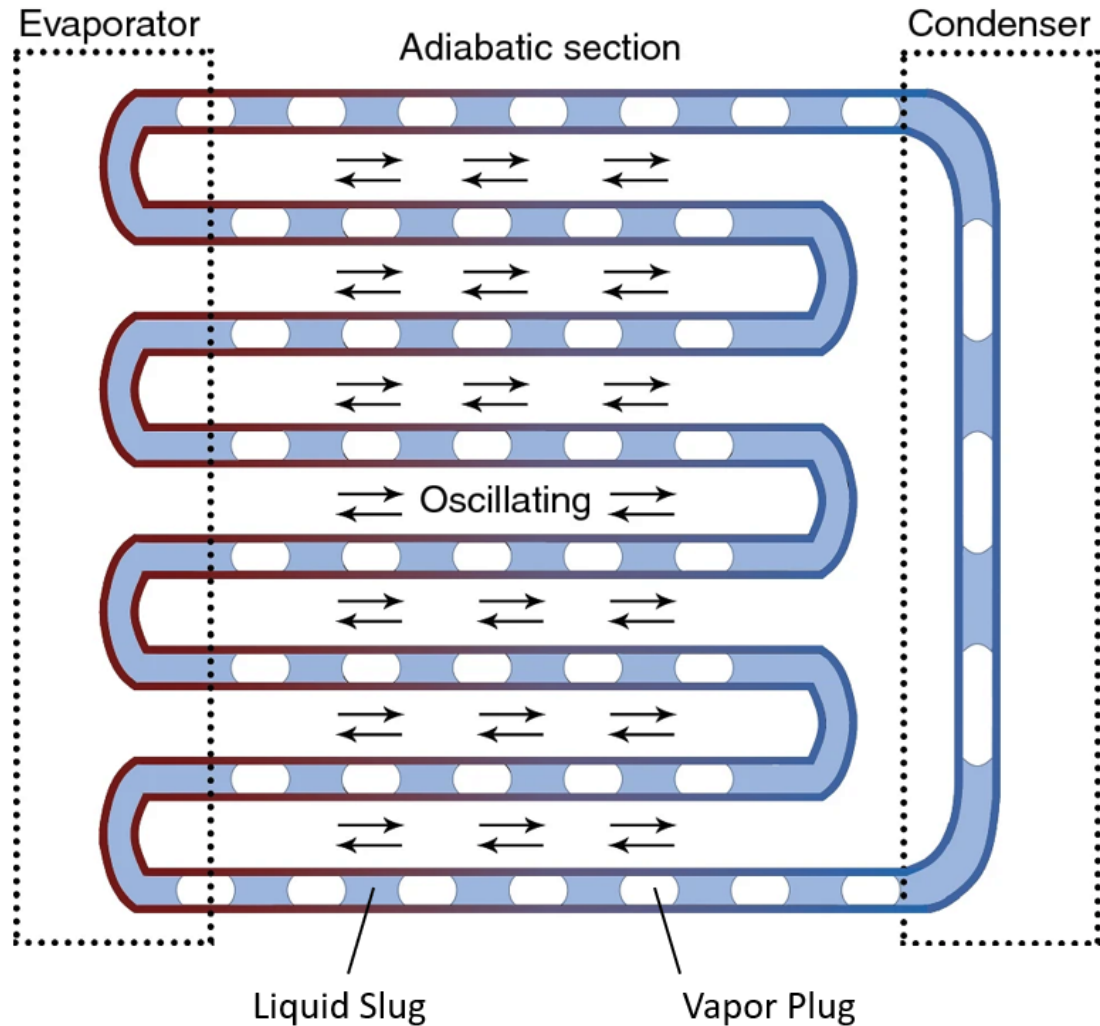


Figure 1: Schematic of an oscillating heat pipe [5].

These devices excel at facilitating energy transport from a heat source to a heat sink, and on the macro scale are used for many different applications, ranging from aerospace to HVAC systems. They have several key advantages over traditional heat pipes. One is that they do not require a porous wick structure to operate, which can add manufacturing complexity and increase costs. A side effect of this is that the liquid flow and vapor flow do not interfere with one another because both phases flow in the same direction. Another is that OHPs are able to be configured into more complex geometries as long as the loop structure is maintained, as compared to a heat pipe, which can typically only operate as a straight length of pipe. This allows for efficient energy transport in systems with more complex or irregular geometries. However, the greatest advantage of OHPs is that as input power increases, so too does their heat transport capability, due to enhanced oscillatory motion and more vigorous phase-change cycling [6].

Miniaturization of OHPs has the potential to significantly enhance thermal management in microelectronic systems. Micro-scale oscillating heat pipes (MOHPs) can leverage their small cross-sectional dimensions to integrate directly with semiconductor devices, facilitating heat transport over extended lengths despite the confined geometry. This capability is particularly advantageous in applications where heat must be removed from densely packed regions and delivered to remote cooling units.

This thesis investigates three specific design enhancements aimed at improving the performance and operational stability of MOHPs. The first approach involves implementing alternating channel hydraulic diameters along the length of the device to

promote better fluid circulation and device startup compared to uniform channels. The second approach examines the integration of reentrant structures that are designed to mitigate liquid flooding and serve as persistent nucleation sites for vapor formation. The third approach explores the incorporation of micro-grooved wick structures within the channels to enhance capillary flow capacity and reduce the risk of dry-out.

Through experimentation, this work aims to contribute to the advancement of MOHP technology and its practical application in high-performance electronic cooling systems. By addressing key design challenges and exploring novel enhancements, this research seeks to support the development of efficient and reliable thermal management solutions for the next generation of semiconductor devices.

2. Background

While MOHPs have a great deal of potential, there are a number of problems with them. In this work, we examine potential solutions to three issues. One problem lies in maintaining an idealized flow regime for these devices. An idealized flow regime involves alternating liquid slugs and vapor plugs of similar size that fill the majority of the channel cross section, which will be referred to as controlled flow throughout this work. This is ideal for several reasons. In oscillating heat pipes, maintaining a controlled two-phase flow regime—characterized by well-defined liquid slugs and vapor plugs—can significantly reduce thermal resistance [6, 7, 8, 9]. Structured flow supports consistent evaporation and condensation cycles and allows for stable thermal conduction through alternating fluid regions [10, 11]. In contrast, chaotic or disordered flow can lead to

stagnation zones where fluid motion halts or becomes irregular, disrupting thermal transport and degrading device performance [12, 13]. Another problem we seek to address is dryout. Dryout in the context of OHPs is a condition in which all of the fluid on the evaporator side of the device has already evaporated, and thus cannot continue to expand at rates sufficient to continue to drive flow. When flow stops in this way, the device is essentially rendered less than useless. Because vapor has much lower thermal conductivity than liquid, the loss of convective transport leaves conduction as the dominant mechanism. Under these conditions, the device conducts heat even less efficiently than it did prior to startup, when liquid was still distributed throughout the channels. This can occur when input heat fluxes rise beyond the operating range of the device. The final issue we examine is that start-up can often fail. Usually, this is due to insufficient heat fluxes at the evaporator and condenser that cannot drive the multiphase flow regime [6].

As stated previously, controlled flow is highly desirable and can present significant reductions in thermal resistance. However, controlled flow is very difficult to achieve. Chaotic flow regimes in which vapor bubbles are more interspersed within liquid columns are much more common, but introduce several inefficiencies. Thus, reentrant structures are a potential way to introduce a more controlled flow regime.

Reentrant structures are artificial cavities that are built into channel walls. Their function is to trap vapor or gas. In doing so, a liquid-vapor interface is created. This liquid vapor interface serves a crucial role, in that it allows for liquid molecules at the interface to more easily overcome the effects of surface tension, thereby evaporating at a

lower saturation temperature. This is useful in the sense that reentrant structures can serve as preferential sites for nucleation because the energy barrier for nucleation is lower [14].

Figure 2 illustrates the general operation of such structures. In figure 2(a), vapor is trapped, forming what is known as a vapor seed. As heat is added, the vapor seed expands to fill the whole reentrant structure, as shown in figure 2(b). The vapor seed continues to expand into the channel, shown in figure 2(c). Once the vapor is in the channel, it is subject to the forces of bulk fluid motion. At some critical mass of the vapor seed, the forces are strong enough to ultimately detach the vapor overhanging into the channel, which forms a bubble and then continues to flow into the channel, as shown in figure 2(d). The most important thing to note in the operation of these structures is that a segment of the vapor seed is ultimately left behind. This means that these sites can continue to serve as preferential nucleation sites.

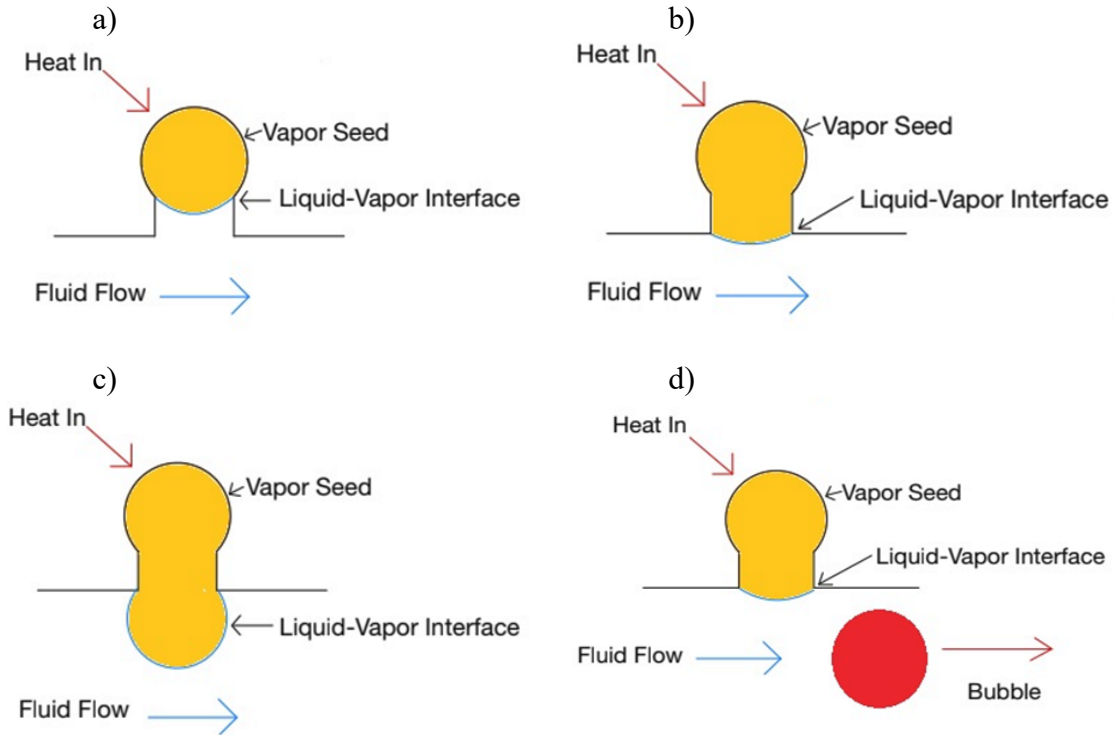


Figure 2: Operation of a reentrant structure. a) Initial vapor seed and liquid vapor interface. b) Gradual expansion of the vapor seed as heat is continuously added. c) Further expansion of the vapor seed into the channel. d) Detachment of vapor bubble into the channel, while the vapor seed is preserved in the cavity.

The benefits of such structures in MOHPs have already been examined, with results indicating that the presence of reentrant structures served to minimize thermal resistance and assist in the startup of these devices [15]. However, achieving these benefits critically depends on the preservation of the vapor seed. Any flooding of the reentrant structures can render them useless. Without the persistent nucleation provided by reentrant structures, bubble spacing becomes erratic, breaking the controlled flow regime. It is this issue that we seek to combat. While maintaining a structured flow

regime is crucial for thermal performance, another major threat to OHP operation is dryout, particularly under high heat flux conditions.

One approach to mitigating the effects of dryout is the use of wick structures. Wick structures serve to enhance capillary forces that can drive the movement of working fluids. Through these structures, capillary action can drive liquid from the condenser side of OHPs to the evaporator side. This imparts some key advantages. Such structures allow for the presence of liquid throughout the entirety of channels within OHPs. This is something that can help to prevent dryout conditions from being reached. Li et al. explored the use of supercapillary structures to create a stable thin film through capillary effects in the case of flow boiling. Figure 3(a) below shows a typical flow boiling regime, in which as heat is added, the fluid progressing from bubbly flow to slug flow to annular flow, and ultimately dryout. In figure 3(b), a cylindrical array of microstructures was fabricated next to the channel walls. By controlling the distance from the walls, as well as controlling the distances between structures and the size of the structures, a capillary structure was created, wherein the fluid was subject to higher capillary pressures. Due to these higher capillary pressures, fluid in the liquid state was driven along the channel walls at flow rates greater than the bulk channel. This ensured that there was always a thin liquid film that would slowly evaporate, thereby staving off dryout [16].

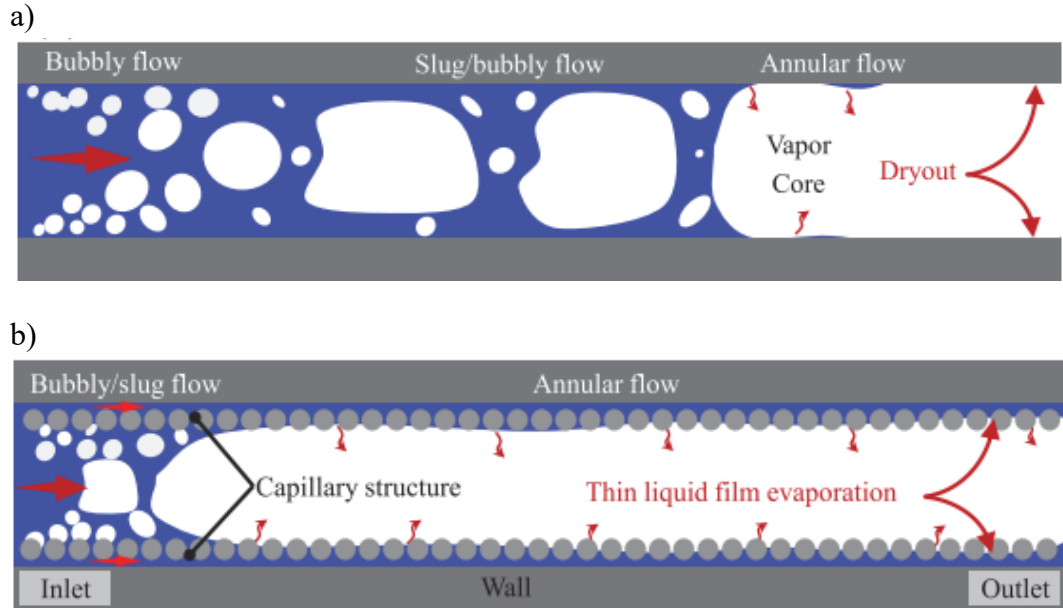


Figure 3: Top down view of flow boiling. a) Progression of different flow regimes through conventional flow boiling. b) Shows the effect of an array of cylindrical microstructures near the channel walls on flow regimes in flow boiling [16].

These cylindrical wick structures arrays present several drawbacks. One is that depending on the exact sizes of each cylinder as well as the etch depth, these can be difficult to fabricate without defects or collapse. It is also more difficult to control the size of the confinement the liquid experiences as it progresses through the cylindrical array, meaning that it is subject to varying capillary forces. Varying capillary forces in the direction of flow can lead to slows or breaks in flow that are highly undesirable. Finally, as the liquid progresses through this structure, it has to ‘hop’ from structure to structure, leading to potential pinning points that can add to the slowed flow effects.

Traditional heat pipes also utilize wick structures as a way to return fluid from the condenser side to the evaporator side of devices. Typically, wick structures utilized in

heat pipes are made from porous materials. Common types of wick structure for heat pipes are made from sintered metal particles or meshed materials. These types of wick structures offer very high capillary forces and high porosity. However, there are several drawbacks to using such structures. Porous materials offer a high degree of tortuosity and flow resistance (in this case, subject to the sizes of particles used to create sintered wicks) and so the return of fluid is greatly slowed. It is also not simple to fabricate and implant such wicks in micro scale devices, and can add significant cost and complexity to devices.

In addition to ensuring continuous liquid presence to prevent dryout, achieving a robust startup is essential for initiating and sustaining two-phase flow. Again, startup issues are typically as a result of insufficient heat fluxes at the evaporator which lead to insufficient driving forces within the device. However, there are ways to utilize device geometry to assist in startup. One method is to alternate the diameter of each straight section of channel in the serpentine loop. While single diameter channels are the standard for most OHPs, dual diameter channels introduce a unique mechanism that enhances the performance of OHPs, particularly during the startup phase and in maintaining an organized flow of vapor bubbles. One of the primary advantages of dual diameter channels is their ability to create imbalanced pressures across the two menisci of vapor bubbles. This pressure differential is crucial during the startup phase of the OHP, as it facilitates the movement of vapor bubbles through the system. The imbalanced pressures can also lead to a more rapid initiation of fluid movement, thereby reducing the time required for the OHP to reach operational stability [17]. The study by Yang et al.

highlights that this pressure imbalance is instrumental in overcoming the initial inertia of the liquid slug, thus promoting a quicker startup.

In addition to aiding in startup, the dual diameter design significantly contributes to the controlled operation of the OHP. As vapor bubbles expand, they are naturally directed into the wider channels, which have comparatively lower flow resistance than the narrower channels. Conversely, when vapor bubbles contract, they are channeled into the narrower sections. This controlled operation is critical for maintaining low thermal resistance within the system. By ensuring that vapor bubbles are efficiently routed through the appropriate channel sizes, the dual diameter design promotes a more controlled flow, effectively reducing thermal resistance, thereby enhancing the overall thermal performance of the OHP [18]. The ability to manage the flow of vapor and liquid phases in this manner is a significant advancement over traditional single diameter designs, which can suffer from increased thermal resistance due to more chaotic flow regimes in which vapor and liquid may be more interspersed. In conclusion, the adoption of dual diameter channels in OHPs presents substantial advantages in both startup efficiency and operational order. The imbalanced pressures generated by the dual diameters facilitate a quicker startup, while the strategic routing of vapor bubbles through appropriately sized channels minimizes thermal resistance.

In summary, while micro oscillating heat pipes offer significant promise for efficient thermal management, several key challenges must be addressed to realize their full potential. Maintaining a controlled two-phase flow regime, preventing dryout in the evaporator, and ensuring reliable startup behavior are critical to device performance.

Prior work has explored approaches such as reentrant structures for nucleation control, wick structures for fluid management, and dual-diameter channel geometries for startup assistance. Building on these insights, the following section describes the design strategies employed in this work to integrate and optimize these enhancements within new OHP devices.

3. Device Design

Given the problems outlined in the prior section, our solutions are as follows. To ensure a controlled flow regime, we examine the use of mushroom shaped reentrant structures that are resistant to flooding and can thus serve as continuous nucleation sites. To mitigate the potential for dryout, we examine the addition of an array of micro groove structures to function as wick structures. To solve the issue of start-up difficulties, we examine channels with varying hydraulic diameters.

a. Mushroom Shaped Reentrant Structures

As previously mentioned, the idea of using reentrant structures to ensure a controlled flow regime can only work if reentrant structures are used as continuous sites of bubble nucleation. This cannot happen if the structures are prone to flooding. As such, we examine mushroom shaped reentrant structures which are immune to flooding effects.

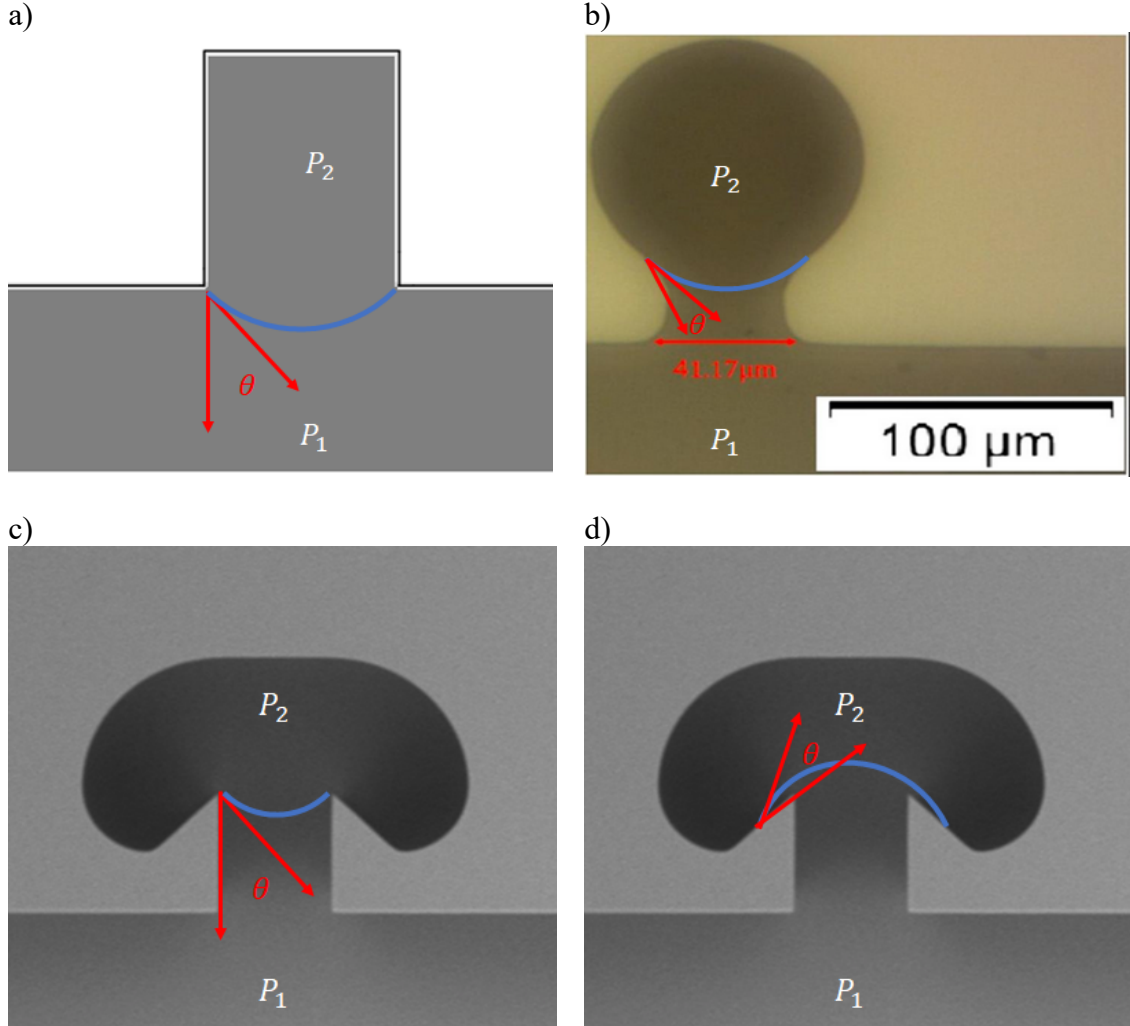


Figure 4: Compares different types of cavities. a) Rectangular cavities that are prone to flooding. b) Optical image of circular cavities in which flooding is ambiguous [15] c) SEM image of mushroom shaped cavities that can only fill to the point the meniscus is drawn. d) Depiction of the ‘flipping’ of the meniscus that would need to happen for mushroom shaped cavities to flood which cannot occur.

To truly understand why the mushroom shaped reentrant structures are flood resistant, we turn to the formula for capillary pressure where P_c is capillary pressure, σ is surface tension, θ is contact angle which is a material property based on the fluid and wall material and thus constant, and R is radius of the cavity.

$$P_c = \frac{2\sigma\cos(\theta)}{R} \quad (1)$$

In figure 4(a), a baseline case of a rectangular cavity is considered. Here, the contact angle between the liquid, solid and vapor is small, while surface tension and radius are constant. Because of the small contact angle, P_c will be high compared to the vapor pressure on the other side of the meniscus. As such, the liquid will be driven into the cavity, destroying the vapor seed in the process. In figure 4(b) the circular cavity is considered. The contact angle is small, while the radius varies. As such, this is an ambiguous case, in which no flooding, partial flooding, or full flooding of the structure are all possible, subject entirely to the exact geometry of the structure. Figure 4(c) shows the mushroom shaped reentrant cavity. The ‘stalk’ of the mushroom fills in much the same way as the rectangular cavity would, due to small contact angle contributing to a high capillary pressure. However, once the head of the mushroom is reached and the geometry undergoes a sharp change, the meniscus can no longer continue to advance. This is because the contact angle must be maintained as the meniscus advances. In order for the contact angle to be maintained, the meniscus would have to invert, as shown in figure 4(d). For that inversion to happen, the capillary pressure would have to be significantly higher than the vapor pressure, to a degree that it cannot achieve naturally, especially without the presence of a pump. As such, the meniscus becomes effectively pinned at the corner where the head of the mushroom begins. Because of this, it is possible to ensure the constant presence of a vapor seed, which allows for continued usage of the structure as a preferential nucleation site. Again, this in turn prevents bubble

spacing and formation from becoming erratic, which would break the controlled flow regime.

b. Micro-Grooved Wick Structures

Micro-grooved wick structures offer a promising means of enhancing liquid return within MOHPs while minimizing flow resistance. Unlike cylindrical microstructure arrays or porous wick structures, micro grooves do not have a varying cross section, the liquid is under the same confinement throughout the entire micro groove. This uniformity means capillary pressures are the same throughout these structures and so there are no undesirable limitations such as localized flow slowdowns or contact line pinning. Additionally, the well structured nature of micro grooves enables efficient phase separation - vapor, when in the form of vapor plugs, is not going to enter the micro groove structures which are filled with liquid at all times. In other words, due to narrow cross sections and consistent liquid confinement, microgrooves are theoretically inaccessible to vapor plugs, ensuring the preservation of continuous liquid pathways through the structure up until the evaporator side of the device. This is in contrast to sintered wicks, in which bubble entrapment can occur and lead to significant performance losses [19, 20].

From a fabrication standpoint, micro grooves also present a practical advantage. They can be manufactured easily and with greater dimensional control than either cylindrical arrays or porous wick structures, reducing both complexity and defect rates. However, because the grooves are open to the channel, the potential for shear.

c. Dual Diameter vs. Single Diameter Channels

Dual-diameter channel configurations are known to facilitate faster startup in MOHPs by creating natural pressure differentials between expanding and contracting vapor plugs. In this study, we extend this concept by integrating dual diameter channels alongside reentrant and microgrooved wick structures — a combination not previously explored. Because of the tendency of dual diameter channels to route expanding vapor plugs into larger channels, liquid and vapor both flow from the evaporator to the condenser. This may affect the operation of both reentrant structures and wick structures. Bubbles forming in reentrant structures placed in smaller channels will inevitably have a tendency to expand, and so there is a question of the impact of that expansion on the routing of fluid flow. Similarly, wick structures are meant to bring liquid from the condenser to the evaporator, but because our micro grooves are open to the broader channel, there will inevitably be opposing shear forces between the ‘bulk’ fluid flow and the fluid in the micro grooves which may limit the efficacy of both the dual diameter channels and the wick structures. These complex interactions raise important questions about whether dual-diameter designs can synergize with wick and reentrant structures to improve performance, or whether they introduce new inefficiencies.

In figure 5 below, a portion of one channel of both a dual diameter and a single diameter device are shown. Dual diameter devices alternate between channel widths of $750\ \mu\text{m}$ and $250\ \mu\text{m}$, while single diameter devices utilize a uniform diameter of $750\ \mu\text{m}$.

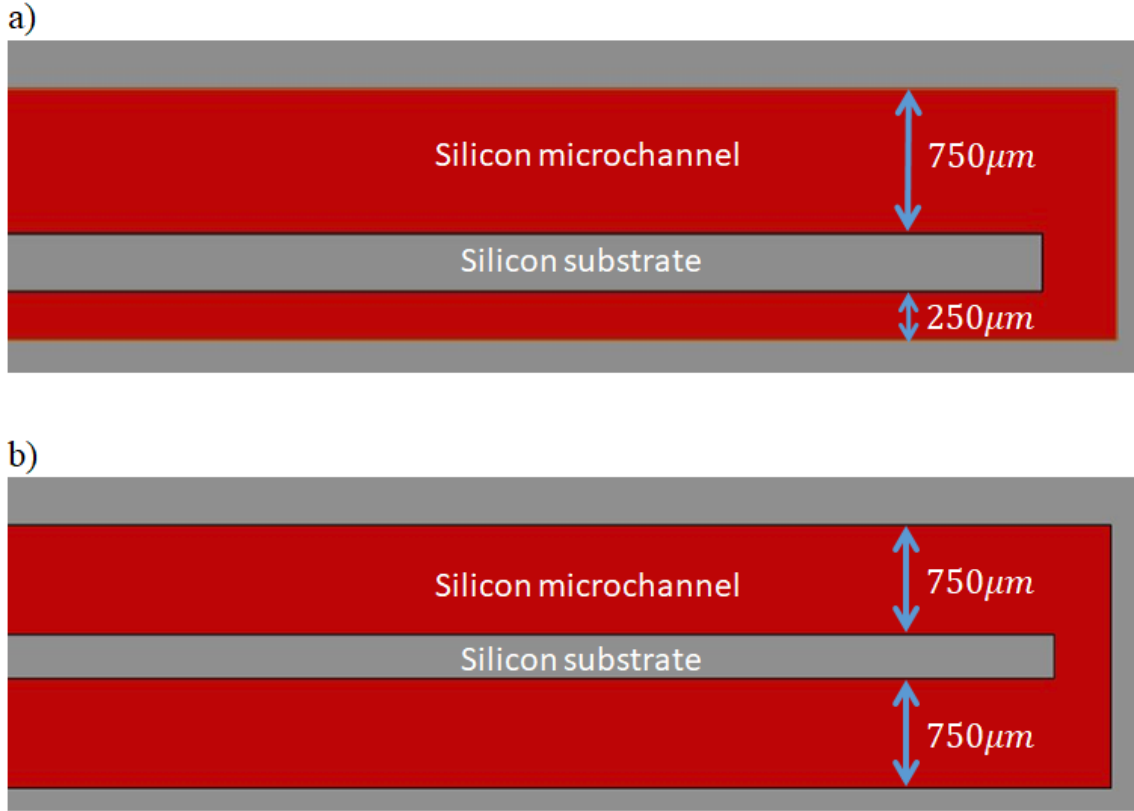


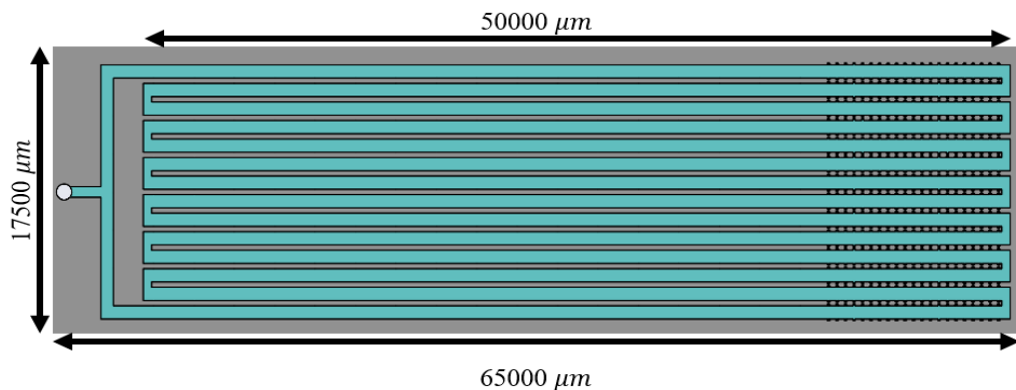
Figure 5: Schematic showing two devices at the turn in one channel. a) Double diameter channel. b) Single diameter channel.

d. Design Cases

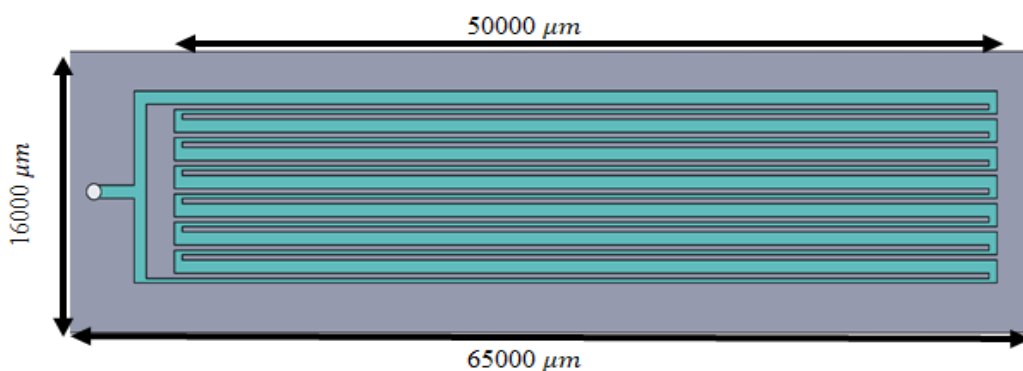
We consider six total design cases. These are the single and the dual diameter cases with no microstructures, the single and dual diameter cases with reentrant structures, and the single and dual diameter cases with reentrant structures and wick structures. We do not consider wick structures on their own. This decision is based on the fact that reentrant structures dictate where nucleation occurs, while wick structures support liquid return to the evaporator side; although both affect device performance, they operate through independent mechanisms. As such, excluding the wick-only case reduces fabrication cost and time.

Our devices are structured to have seven turns, with channels that are 50,000 μm in length. An example of the single diameter reentrant case is shown below in figure 6(a) while an example of the dual diameter baseline case is shown in figure 6(b). Figure 6(c) shows the reentrant structure array. The depth of our channels is typically between 200 and 250 μm as shown in figure 6(d) below. Reentrant structure openings are 40 μm in width as shown in figure 6(c), and reentrant structures are etched to depths slightly smaller than channel depths. This is an unintended side effect of the fact that channels and reentrant structures are etched together, and the significantly smaller confinement of the structures slows etching rates in deep reactive ion etching. Our wick structure devices are also made from silicon and glass, though the glass itself is etched with arrays of 10 $\mu\text{m} \times 10 \mu\text{m}$ cross section channels that are 50,000 μm in length. Width of single diameter device chips was 17500 μm , while dual diameter device chip width was 16000 μm . Number of wick structures per channel varies based on channel width. For channels with widths of 750 μm , there are 10 wick structures. For channels with widths of 250 μm , there are 3 wick structures. Spacing between wick structures is 50 μm .

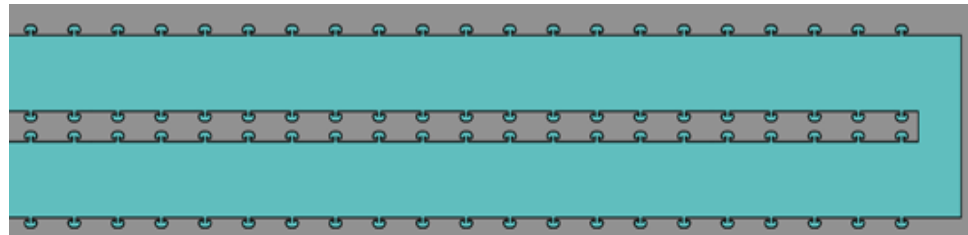
a)



b)



c)



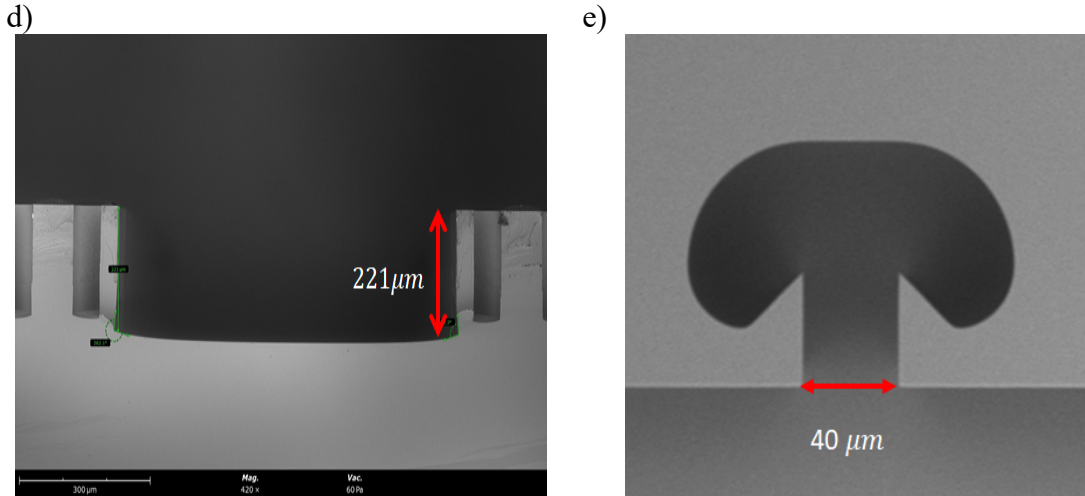


Figure 6: a) Rendering of a single diameter device with the reentrant structure array. b) Rendering of a dual diameter device. c) SEM image of the channel cross section, etched to a depth of 221 microns. c) SEM image of a single reentrant structure with a top down view. d) Rendering of the wick structure array in a single channel.

4. Fabrication

Fabrication begins with a silicon wafer that was patterned twice: once for the through-holes (reservoir structures) and once for the OHP channel patterns. Each patterning process involves three core steps:

1. **Photoresist Coating:** A uniform layer of photoresist (AZ10XT) is spin-coated onto the silicon substrate with a thickness of 11 microns.
2. **Lithography:** UV lithography is used to transfer the desired pattern onto the photoresist using the Heidelberg MLA 150. The pattern is then developed using AZ 400K developer.

3. **Etching:** The exposed silicon areas are etched using deep reactive ion etching (DRIE) to define either the through-holes or the channel structures. DRIE is done using the Oxford PlasmaPro 100 Estrelas.

This two-step patterning is necessary to independently define large-area through-holes and finer-scale channel features. Through-holes are patterned on the unpolished side of silicon wafers, while channel geometries (including reentrant structures) are patterned on the polished side.

To create the wick structures, borosilicate glass wafers with deposited layers of silicon on the top and bottom are treated similarly. Silicon is patterned then etched through reactive ion etching (RIE). Remaining silicon serves as a hard mask for wet etching done with hydrofluoric acid (HF) to etch the glass. Afterwards, tetramethylammonium hydroxide (TMAH) is used to remove the remaining silicon. For devices without wick structures, we simply use unprocessed plain borosilicate glass wafers.

Once both glass and silicon wafers were processed, both are cut into chips using an automated dicing saw, then cleaned in a piranha solution. Silicon and glass chips are then bonded together using anodic bonding [21]. Although anodic bonding provides strong, hermetic seals, it is difficult to align wick structures and silicon chips appropriately. Because of these difficulties, silicon and glass chips with wick structures are bonded using PDMS as an adhesive via the stamp and stick method [22], which is then sealed on the sides with epoxy to create a hermetic seal. Figure 7 below shows a simple schematic of fabrication utilizing 2D cross sections of wafers.

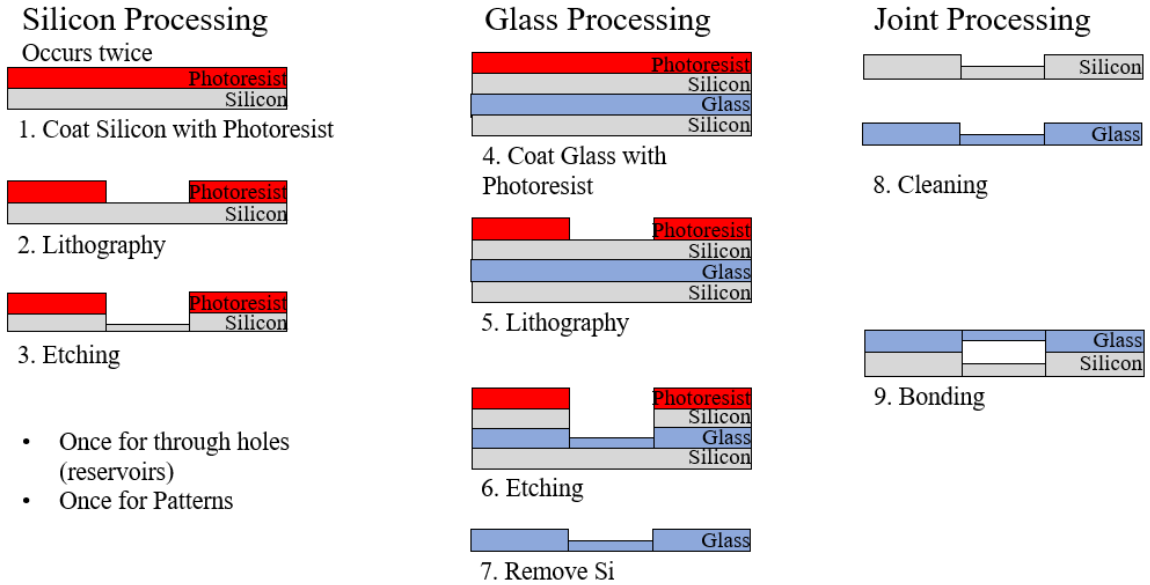


Figure 7: Fabrication steps for silicon and glass wafers in 2D.

5. Experimental Design

a. Device Filling

A key challenge in MOHP experimentation is properly filling the device with working fluid while minimizing the presence of non-condensable gases. Proper filling not only affects startup reliability and sustained oscillation, but also plays a major role in enabling consistent comparisons across design cases. Below, we describe multiple filling methods explored during this work, including their outcomes and limitations.

Devices are ideally filled with degassed fluid. Non condensable gases mixed into the fluid can influence the performance of the device. Additionally, non condensable gases like air already present in the device should be controlled for. We tested four different filling setups. Although some of these setups proved nonviable, we include

discussion of all four to document the design rationale and the constraints encountered, which helped to inform future filling improvements.

i. Filling Setup 1

The first setup is not operational, but would have produced a desirable result. For this setup, we use a specialized custom setup to fill the device, shown in figure 8. This system consists of a vacuum pump which is connected to a fluid container that sits on a hot plate and the device through a line system. The device itself is connected to the line system through a glass capillary tube that is bonded to the device with heat resistant epoxy.

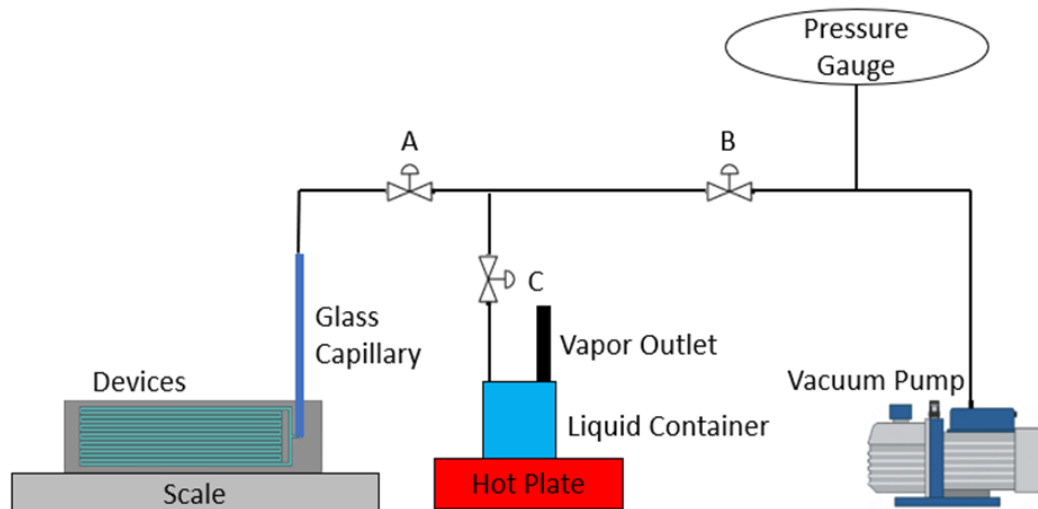


Figure 8: Shows the first setup used for device filling.

The filling process for this setup begins with valve C closed, valves A and B open, and both the vacuum pump and the hot plate on. The device is pumped down to a low pressure, approximately 2000 mTorr. The fluid boils on the hot plate, allowing mixed

in gases to escape. Once the fluid has been degassed, valve A is closed and valve C is opened briefly while the vacuum pump is still on. This is to vacuum any air out of the line. Valve B is then closed, while valve A is opened. Because the device is at a pressure lower than atmospheric pressure, while the fluid container is open to the atmosphere through the vapor outlet, there exists a pressure gradient that serves to drive degassed fluid into the device. The device itself sits on a fine scale that is accurate to within 10^{-5} grams. This allows us to control the mass of working fluid in the device. We use deionized water as the working fluid, and so density is known. As a result, we can calculate the volume of fluid within the device. The percent volume of fluid in the device is known as the filling ratio. Filling ratio is a very important detail in OHPs as the amount of fluid in the device can affect both the fluid motion and heat transfer characteristics of OHPs [6]. Typically, filling ratios of 40% to 60% are used in OHPs. In our devices, we target filling ratios of 50%. Once our devices are appropriately filled, we seal them by melting the glass capillary tube that attaches them to the line system.

Unfortunately, this setup had far too many issues to be viable. By far the largest issue was in dealing with the glass capillary. In order to be able to safely melt these capillaries in such a way that they would form a good seal, we had to use very thin glass capillaries. Diameter of the capillaries used was 1 mm, with a wall thickness of 0.1 mm. Because of the way these capillaries were manufactured, the ends of them were sealed, and so to even use them, we had to break off one end, which led to uneven breaks and even more fragility. Once broken, a number of methods were used to attempt to bond the glass capillary to actual devices. Many of these failed, though some did succeed.

However, the other end of the glass capillary had to be attached to the line system and that was the biggest point of failure. Because the capillaries were so thin, it became almost impossible to hook them up to tubing without breaking them. In situations where it was done, we could not seal the connection with epoxy for fear of breaking the capillaries, and so there were leaks in the line system. Because the device filling relied on a pressure gradient that was not driven by a pump, it became impossible to fill the device under such a method. We did try to degas fluid and then fill a syringe, then use a syringe pump with our line system, but this proved to be unreliable and difficult to control. Due to time constraints, we ultimately abandoned this setup in favor of a much simpler one.

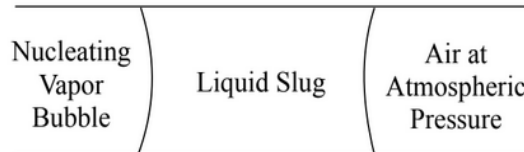
ii. Filling Setup 2

The second filling setup utilized was simply filling a syringe with degassed fluid, then filling the device directly with that syringe. This had a number of obvious flaws. The first is that while we may have degassed the fluid, there were a number of opportunities for air to diffuse back into the fluid. We did not control for air in the actual device, and so there were inevitably non condensable gases mixed into our fluid. However, this method was much easier to use and produced devices that could be tested, allowing us to move onto experimentation. Given that all devices were filled under the same conditions, this was initially deemed to be acceptable since we sought to show improvement over our own baseline cases. Unfortunately, testing these devices yielded extremely poor results. By having air initially at atmospheric pressure inside our devices, we effectively raised the internal pressure, increasing the vapor pressure threshold needed for bubble

nucleation and subsequent fluid movement. A schematic is shown below in figure 9(a).

We found that even at the highest heat fluxes we were capable of reaching, this could at best produce a quasi-static equilibrium where liquid slugs were more or less oscillating in place, as shown in figure 9(b). These conditions prevented normal operating behavior, limiting our ability to draw meaningful performance comparisons across design cases.

a)



b)

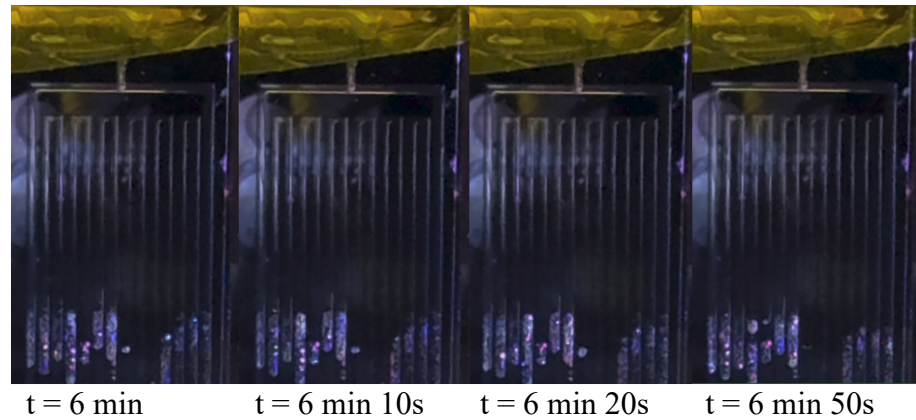


Figure 9: a) Shows a schematic of pressures across the liquid slug. The nucleating vapor bubble pressure was roughly equal to the air pressure on the other side, causing a static equilibrium in which the liquid slug did not move. b) Frames of an OHP during experimentation at different time stamps illustrating this effect.

iii. Filling Setup 3

Following this, we went back to our original approach with some modifications. First, instead of relying on a passive pressure gradient, we degassed fluid by boiling it, then filled a syringe and used a syringe pump to drive fluid into the line system. Second, we abandoned the glass capillary tubes and instead used plastic tubing, which we then melted with a lighter. This approach is less robust than using glass capillaries, but also much less difficult to use. After melting the plastic tubing, we then sealed it with epoxy. Initially, this setup still had a significant problem in that the vacuum pressures we were using were too low. This meant that as water came close to entering the devices, liquid would flash evaporate into vapor, creating a significant localized pressure increase where we could not continue to push liquid into the device without first overcoming the energy barrier necessary to condense vapor back into liquid. However, we were able to overcome this by introducing small leaks in the line system intermittently. In doing so, we ensured that air pressures were sufficiently high to prevent flash evaporation, while low enough that our devices could at least operate, though likely at a limited efficacy compared to filling under a ‘true’ vacuum pressure. A schematic of this setup is shown below in Figure 10.

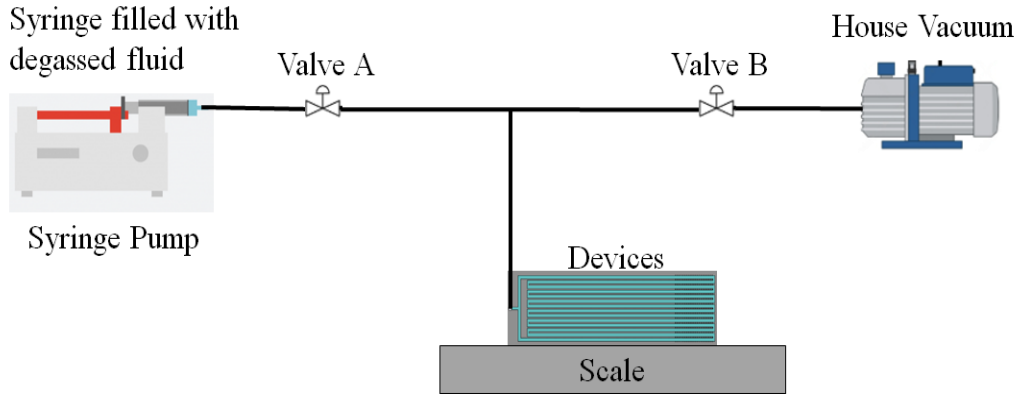


Figure 10: Schematic of the third filling setup.

iv. Filling Setup 4

The final filling setup we tested relied on a modification to our devices in which instead of a single reservoir, we had two on opposite sides of the device as shown below. One was connected to the syringe via plastic tubing, and the other was connected to a weak vacuum. In utilizing this setup, it became possible to easily alternate between vacuum and pumping in liquid by utilizing valves, allowing us to remove vapor from the device even as liquid would enter, thereby eliminating the localized pressure increase caused by flash evaporation. This also had the advantage of drawing liquid towards the center sections of the device, which in all other filling setups was difficult to do. This setup was by far the most effective of the ones we tested. However, it also required all new devices, which we did not have time to implement. The modified devices and a schematic of the filling setup are shown below in figure 11.

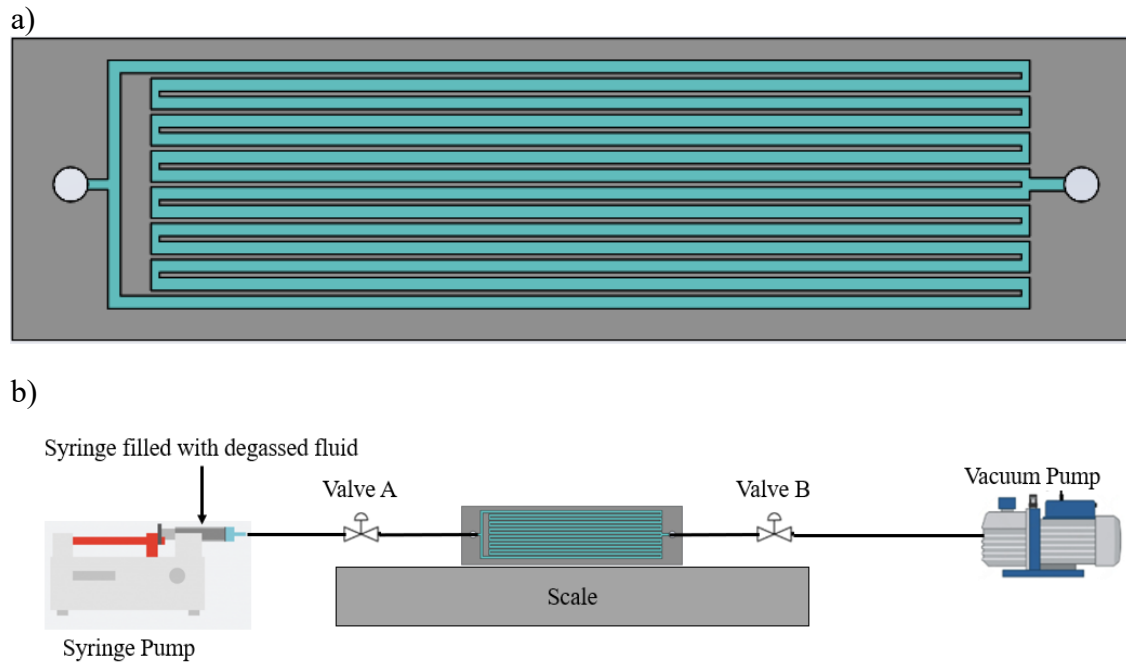


Figure 11: a) Modified devices with two reservoirs. b) Schematic of fourth filling setup.

b. Experimental Setup

To evaluate the performance of these devices, a custom experimental setup was designed and implemented. A schematic of our experimental setup is shown below in figure 12.

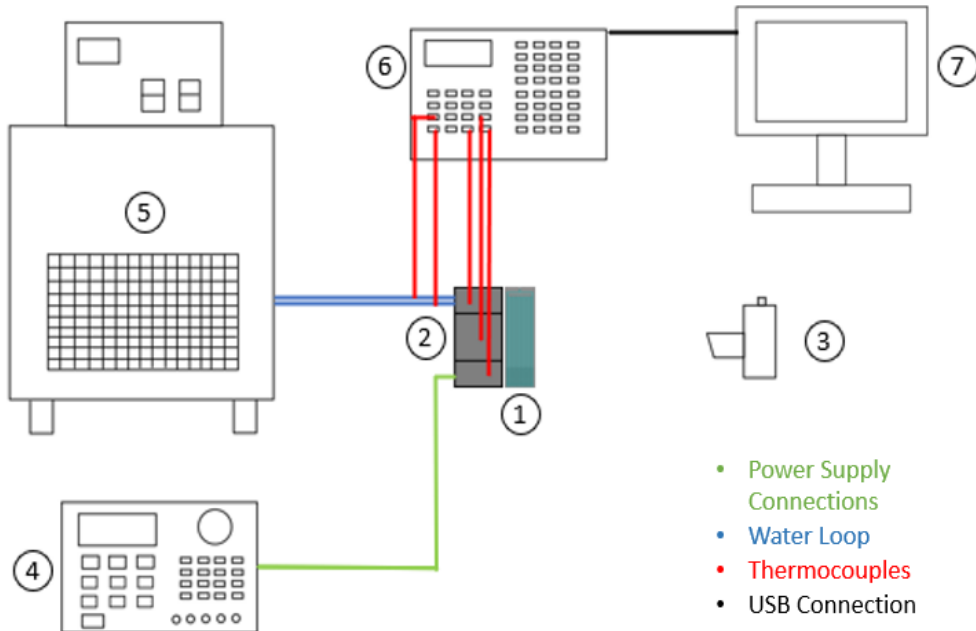


Figure 12: Schematic of the experimental setup. 1) The device. 2) Evaporator, adiabatic section and condenser housing. 3) Camera. 4) Power supply (Tektronix PWS4602). 5) Recirculating chiller (VEVOR 6L Laboratory Chiller Circulator). 6) Data acquisition unit (Agilent 34972A) 7) PC.

The device sits on a custom built testing setup oriented vertically and video is taken with a camera. The testing setup consists of a walnut wood block with two cavities in which two copper blocks sit, shown more closely in figure 13.

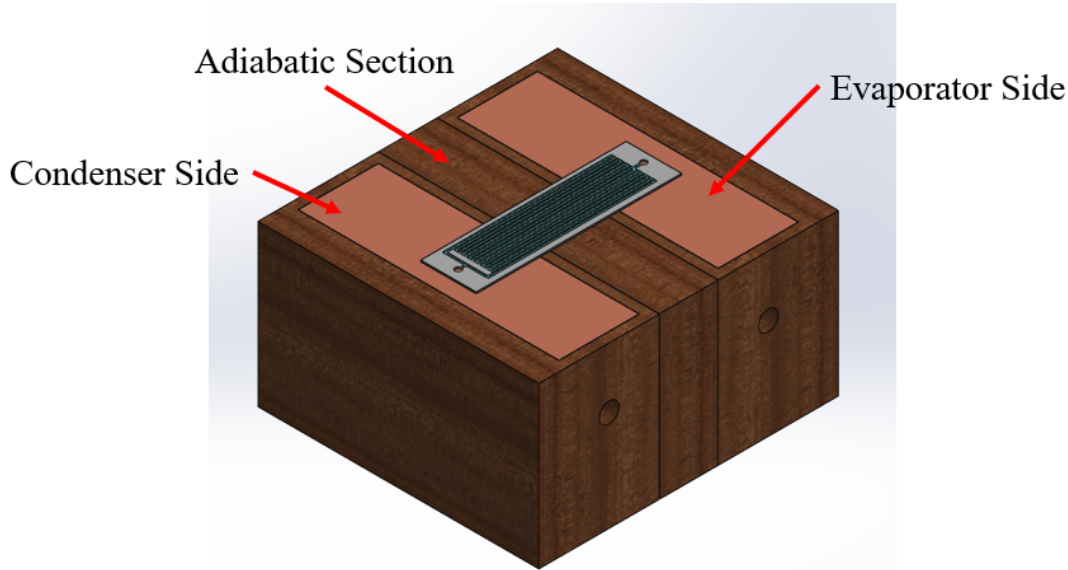


Figure 13: Rendering of the evaporator and condenser housing.

Walnut is used as insulation due to its exceptionally low thermal conductivity of approximately $0.04 \frac{W}{m \cdot K}$. The copper blocks serve as an evaporator and condenser. Copper is used due to its high thermal conductivity of approximately $400 \frac{W}{m \cdot K}$. The evaporator has a hole in which a cartridge heater can be slotted into. The cartridge heater is powered by an external power supply unit. The condenser has a water loop running through it. The temperature of the water at the input to the condenser is set by a recirculating chiller. The chiller has a built in pump that circulates fluid at $6 \frac{L}{min}$ through a $\frac{3}{8}$ inch tube. Thermocouples run from a data acquisition system and are placed at five points: the evaporator, the condenser, the adiabatic section, and the inlet and outlet of the water loop on the condenser. The data acquisition unit is connected to a PC to easily record data.

c. Methodology

Input power to the evaporator can be calculated as shown in equation 2 below, where Q_{evap} is the heat flux, V is voltage and I is current.

$$Q_{evap} = VI \quad (2)$$

By taking the temperatures at the inlet and outlet of the condenser, the output heat flux from the condenser can be calculated as follows:

$$Q_{cond}(t) = \dot{m}c_p(T_{out}(t) - T_{in}(t)) \quad (3)$$

It then becomes possible to account for any losses in the system using conservation laws.

It is important to note that to get this temperature difference, we installed a valve in the tubing of the chiller to limit the mass flow rate of the fluid, as we found the default volumetric flow rate of $100 \frac{mL}{sec}$ to result in too significant of a flow rate to be able to quantify a temperature difference no matter how efficient our device was. As such, fluid flow rates were approximated by running the chiller with one end disconnected such that it was filling a beaker of known volume, and recording the time it took for that beaker to fill. The fluid flow rate we found to be acceptable for measurable temperature differences was $3.5 \frac{mL}{sec}$.

We sought to quantify two things in experimentation. The first is thermal efficiency of all of our design cases. Normally efficiency is quantified as follows:

$$\eta_{power} = \frac{Q_{cond}(t)}{Q_{evap}} \quad (4)$$

Where η_{power} is thermal efficiency, Q_{evap} is total heat supplied to the evaporator side of the device, and Q_{cond} is total heat dissipated by the condenser. However, our input power is more or less steady, while our output power changes with time based on the operation of our devices. As such, to get an absolute measure of efficiency, we instead compare energy as opposed to power by integrating with respect to time, as shown in equation 5 where x is the initial activation time of the device.

$$\eta_{energy} = \frac{\int_x^t Q_{cond} dt}{Q_{evap}*(t-x)} \quad (5)$$

It is important to note that typically, this is not done in the literature. Experimental works typically present either thermal resistance or efficiency of their devices at steady state temperatures. We never achieved a steady state temperature because the duration of our experiments was limited to approximately fifteen minutes under heat. This is because the cartridge heater got hot enough on its surface that it approached the auto ignition temperature of our experimental setup, which forced us to stop our experiments before reaching steady state. Additionally, we do not present thermal resistance because it is a more unstable metric in the transient sense. Thermal resistance is a ratio of the temperature difference to the heat dissipated. In the early stages of each experiment, heat dissipated is small, and stays small for a much longer time than the temperature difference. Due to this and noise in temperature data, thermal resistance has a tendency to fluctuate by several orders of magnitude. In the later stages of each experiment, thermal resistance continues to exhibit smaller fluctuations by one order of magnitude due to noise in temperature data. Because of this, we felt it did not make sense to present the

transient evolution of thermal resistance as a way to quantify device performance over time.

The other characteristic we wanted to measure was the input heat flux at which dryout conditions can occur in these devices. In comparing the case of wick structures to the baseline cases, we can observe if the wick structures have any tangible effect on raising the operational limit of these devices. This is something that we did not measure in our current experiments due to time constraints. However, sweeps of input heat fluxes will be done in future experiments.

6. Results

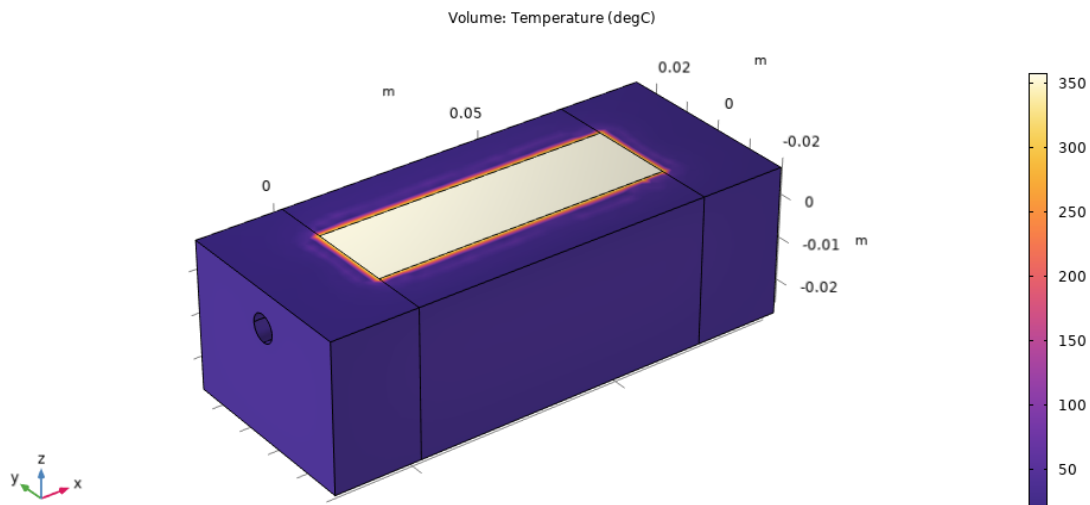
Due to extensive delays in fabrication, as well as difficulties with filling, only one round of experimentation was possible. For this initial set of experiments, we examined the transient response of these devices over a period of fifteen minutes under a constant heat flux. The input from the power supply was 60V and a current of 1.2A, corresponding to a total power of 72W.

We ran a steady state simulation in COMSOL of our experimental setup to understand the power distribution throughout our evaporator, and to understand how much power made it to the top surface of the copper block where the device sat. Given that the cross section was uniform throughout the evaporator and the heater was at the center of the copper block, this was essentially a two dimensional conduction problem, and so simulation was an attractive option to quantify the power distribution. The simulation itself was three dimensional for accuracy. We then compared our simulation

results against an experimental trial with no device with a thermocouple on the cartridge heater surface and another on the surface of the copper block to validate simulation data. We found good agreement between temperatures, though we had to extrapolate the steady state temperature data for experimental results as temperatures got too high for our experimental setup to handle safely. A comparison of steady state temperatures across the whole setup and transient temperature data from the heater to the copper block surface can be found in figure 14 below.

Using surface integration in COMSOL, we were able to discover the total power reaching the surface of the copper block at steady state, which read as 52.741W. By using an area ratio of exposed device area to copper block area, we calculated the total heat that each type of device would experience. This is shown in table 1 below.

a)



b)

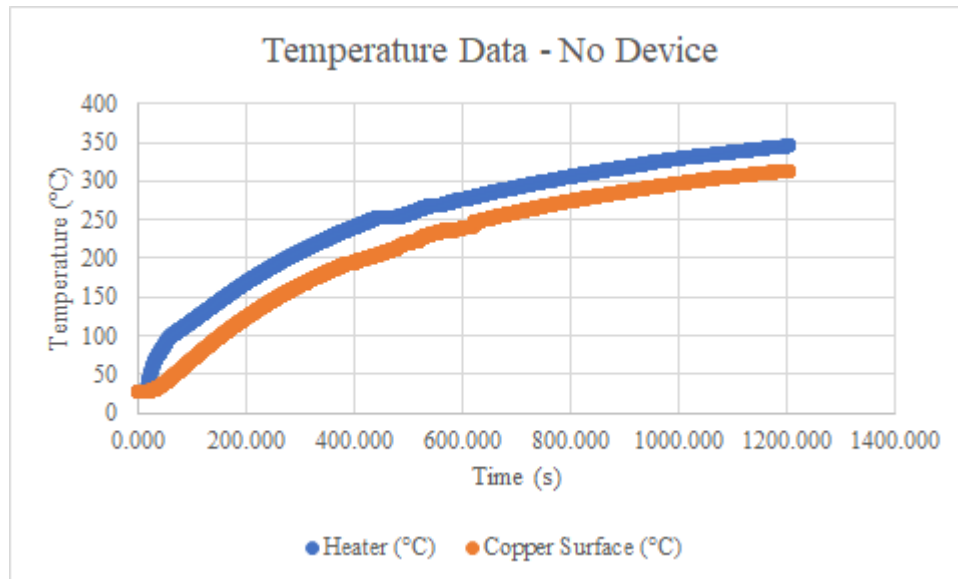


Figure 14: a) Temperature heatmap of evaporator at steady state. b) Experimental data over time for cartridge heater and copper block surface.

Total Heat through Copper Surface	52.741 W
Area of Top Surface of Copper Block	.0014 m^2
Area of Single Diameter Device Exposed to Heat	.00036 m^2
Area of Dual Diameter Device Exposed to Heat	.00033 m^2
Total Heat through Single Diameter Device	13.562 W
Total Heat through Dual Diameter Device	12.432 W

Table 1: Total heat calculations for single diameter and dual diameter devices.

We gathered temperature data for all but one of our designs (single diameter reentrant devices broke after we altered the mass flow rate on the water loop so we could not collect temperature data and due to equipment outages we could not make more) and video data for all of our designs. We also gathered temperature data for a baseline conduction case using an unfilled device. Using the temperature data for the inlet and outlet of the water loop running through the condenser, we quantified the total power dissipated by the water loop using equation 3. Using this data, we quantified a transient efficiency as described in equation 4 for all tested devices, shown in figure 15 below, then quantified an energy efficiency as described in equation 5. Energy efficiency is shown in table 2 below.

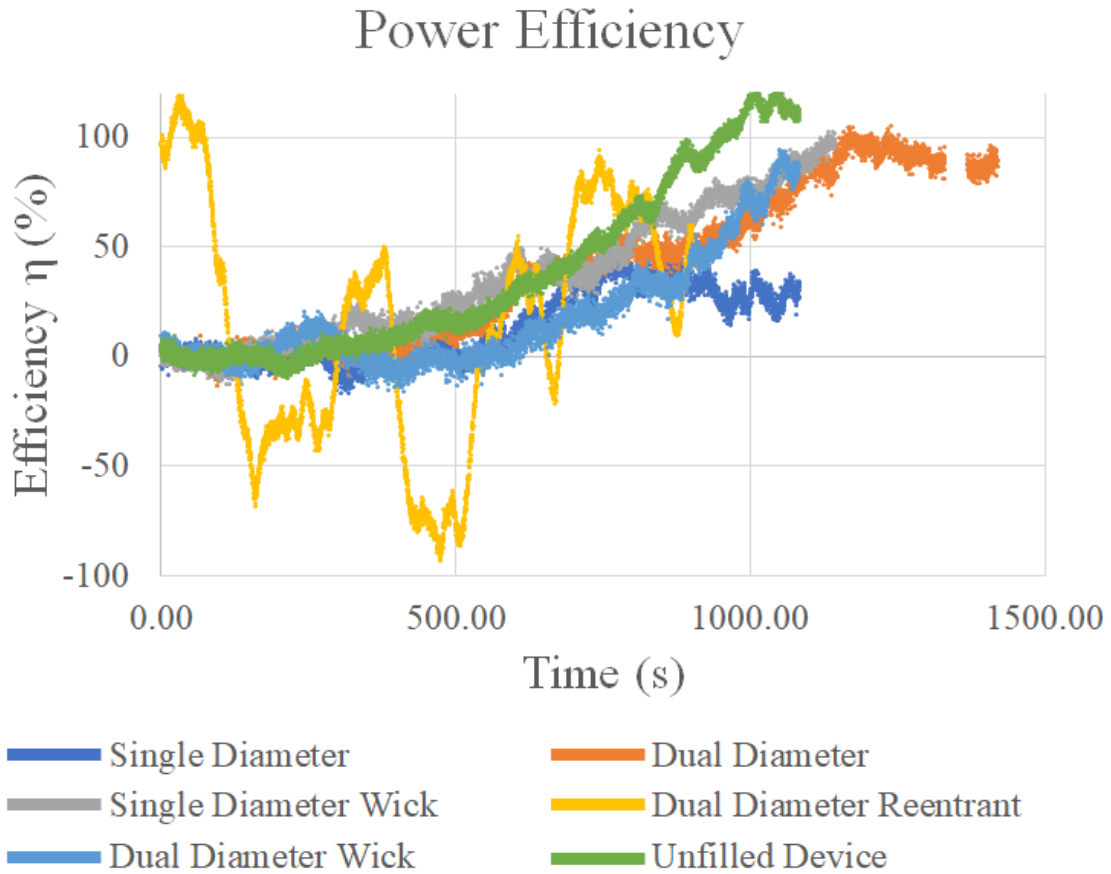


Figure 15: Power efficiency data for all devices with temperature data.

<u>Energy Efficiency</u>	
Single Diameter (leaked during testing)	29.40%
Single Diameter Wick	62.46%
Dual Diameter	57.40%
Dual Diameter Reentrant (leaked during testing)	29.32%
Dual Diameter Wick	39.00%
Unfilled Device	36.92%

Table 2: Table showing energy efficiency for all devices with temperature data.

In the power efficiency graph, there are some devices that show efficiency in excess of 100%. This is likely due to noise in temperature measurements. Our heat dissipation calculation assumes a 3.5 mL/s flow rate of water through the water loop. However, the condenser tubing is designed for a 100 mL/s flow rate. With such a significantly lower flow rate, there are sizable air bubbles in the water loop. Because air has a lower specific heat than water - $1005 \frac{J}{kg \cdot ^\circ C}$ for air compared to $4184 \frac{J}{kg \cdot ^\circ C}$ for water - heat dissipation and energy efficiency should be lower than what is calculated. However, the trends shown in figure 15 above make sense; as more heat is added and devices become more active, efficiency tends to improve. This is consistent with all literature on these devices. Another thing to note about power efficiency; the unfilled device seems to outperform all other devices. This is likely because the unfilled device was not sealed with epoxy. In other words, there was no epoxy on the backside of the unfilled device where it would make contact with the condenser. Epoxy is a polymer, and often has poor thermal conductivity. As such, the performance of the unfilled device is skewed above what it should be. It is also worth noting that there is some variance in the duration of experiments. This is again because of the cartridge heater getting hot enough to burn our experimental setup. Given this, when our setup starts smoking, we stop our experiments. It is also important to emphasize that power efficiency gives glimpses into how performance evolves with time, but it is not an absolute measure of performance. In other words, while certain cases may reach or exceed the performance of others at certain times, this does not necessarily mean those cases performed better overall.

In comparing the results of device trials more closely, we can glean some important and interesting information. In figure 16 below, we examine the single versus dual diameter baseline cases.

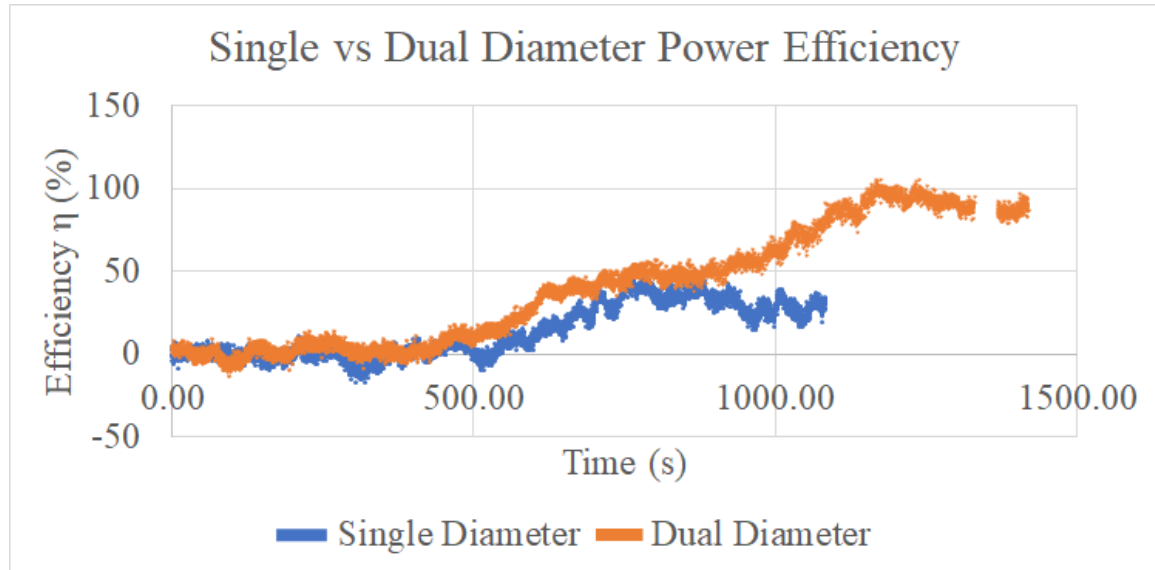


Figure 16: Power efficiency of single vs dual diameter devices.

Cross referencing video data with the above graph, dual diameter devices achieve startup at time $t = 435$ seconds, while single diameter devices achieve startup at time $t = 480$ seconds. It is also important to note that the single diameter device partially leaked at time $t = 580$ seconds, though fluid continued to oscillate even after leakage. Nevertheless, the dual diameter device was able to activate sooner than the single diameter device, which is as expected as outlined in section 2(c). Because the single diameter device leaked, it lost a significant portion of fluid and was less able to resist dryout. The dropoff in performance compared to the dual diameter device at approximately the 800 second mark is likely due to dryout. The dual diameter device was also able to sustain oscillation for a longer period of time than the single diameter device due to the design facilitating

motion through unbalanced pressures. This explains the differences in both power efficiency and overall energy efficiency (single diameter at 29.40% and dual diameter at 57.40%). Furthermore, while we do not have clear confirmation here, it is very likely that due to this, the dual diameter device would have outperformed the single diameter device over the given time frame, even if the single diameter device had not leaked.

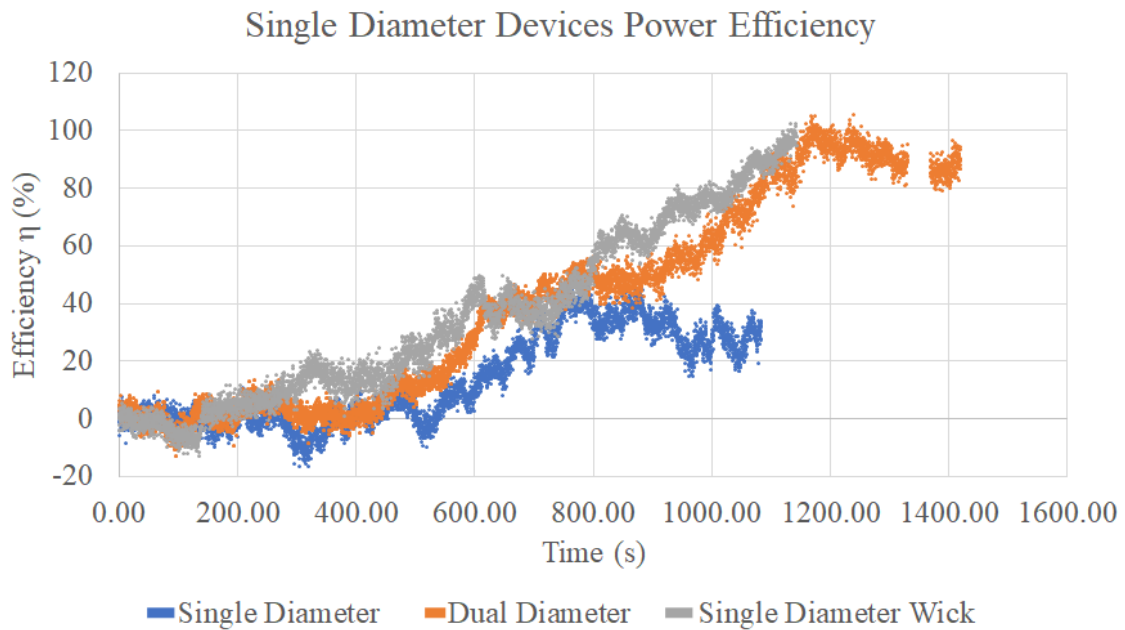


Figure 17: Power efficiency of single diameter devices. This also includes the dual diameter baseline case for comparison.

In figure 17 above, the single diameter wick structure device's efficiency is compared to both the single diameter and dual diameter baseline cases' efficiencies. The dual diameter baseline case is included because the single diameter baseline case seems to track fairly closely with the dual diameter case, and the single diameter case ultimately leaked. As such, comparisons of the single diameter wick structure and the dual diameter cases are worth examining. As shown above, the single diameter wick structure case is

capable of enhanced performance by both power and energy metrics of efficiency.

However, the single diameter wick structure device also shows another improvement; it seems to take a much longer time to reach the same degree of dryout as the dual diameter case, as shown below in figure 18.

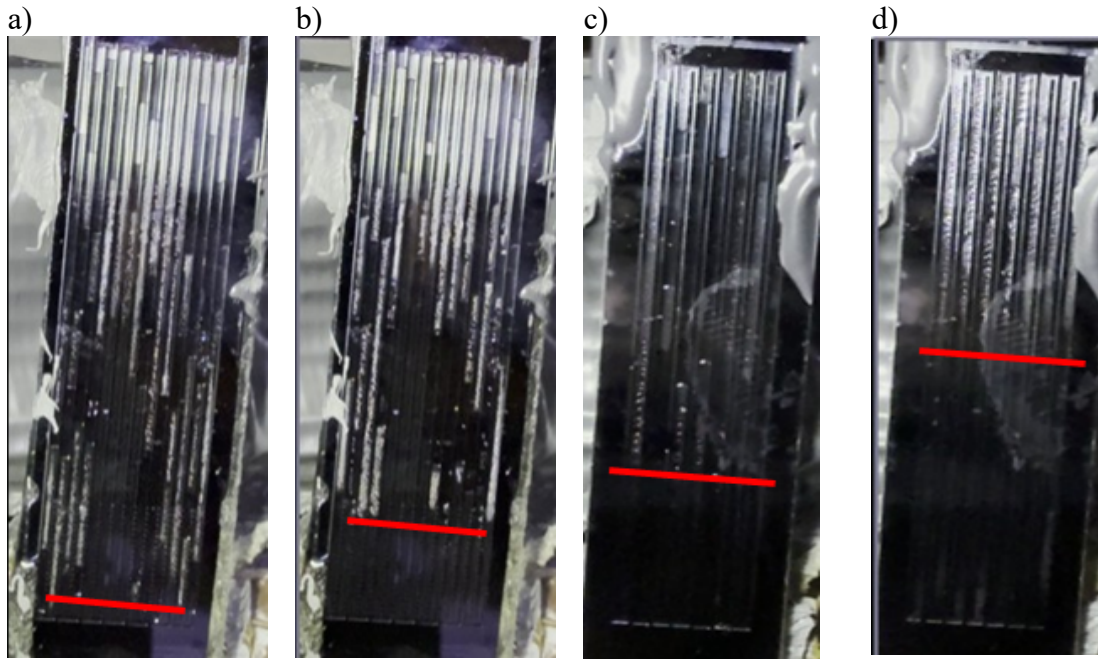


Figure 18: a) Single diameter wick device at $t = 7$ minutes. b) Single diameter wick device at $t = 14$ minutes. c) Dual diameter device at $t = 7$ minutes. d) Dual diameter device at $t = 14$ minutes.

If we think of dryout as a length measurement from the end of the channel on the evaporator side, then at $t = 7$ minutes, the single diameter wick device has experienced virtually no dryout. At $t = 14$ minutes the single diameter wick device shows approximately $\frac{2}{3}$ the dryout that the dual diameter device experienced at $t = 7$ minutes, and $\frac{1}{3}$ the dryout that the dual diameter device experienced at $t = 14$ minutes. Because of this, the single diameter was able to maintain more fluid in the liquid state for longer, and

could thus transport more energy than the dual diameter case, thereby explaining the eventual increase in power efficiency and the higher energy efficiency, with the single diameter wick case at 62.46% and the dual diameter case at 57.40%.

However, this effect is ambiguous. In testing the dual diameter wick structure device, there are several key differences. In figure 19 below, there is a similar comparison between the single diameter wick device and the dual diameter wick device. When taking the distance from the end of each channel to the dryout line, the dual diameter wick device seems to perform significantly worse in terms of dryout mitigation than the single diameter, though it is slightly better than the baseline dual diameter case. Also, the dual diameter wick device never actually achieved startup. There are several different potential explanations for this. The first is that there is a crack in the glass on the device. We sealed this crack with epoxy, but it may be that the sealing is imperfect, and so the device is at atmospheric pressure which we already saw can influence whether or not the device can start up. The second is that the device never actually achieved startup because our hypothesis on the interaction between capillary flows and flow in broader channels producing an opposite shear is correct, which could potentially make it significantly more difficult for nucleating bubbles to be able to push fluid.

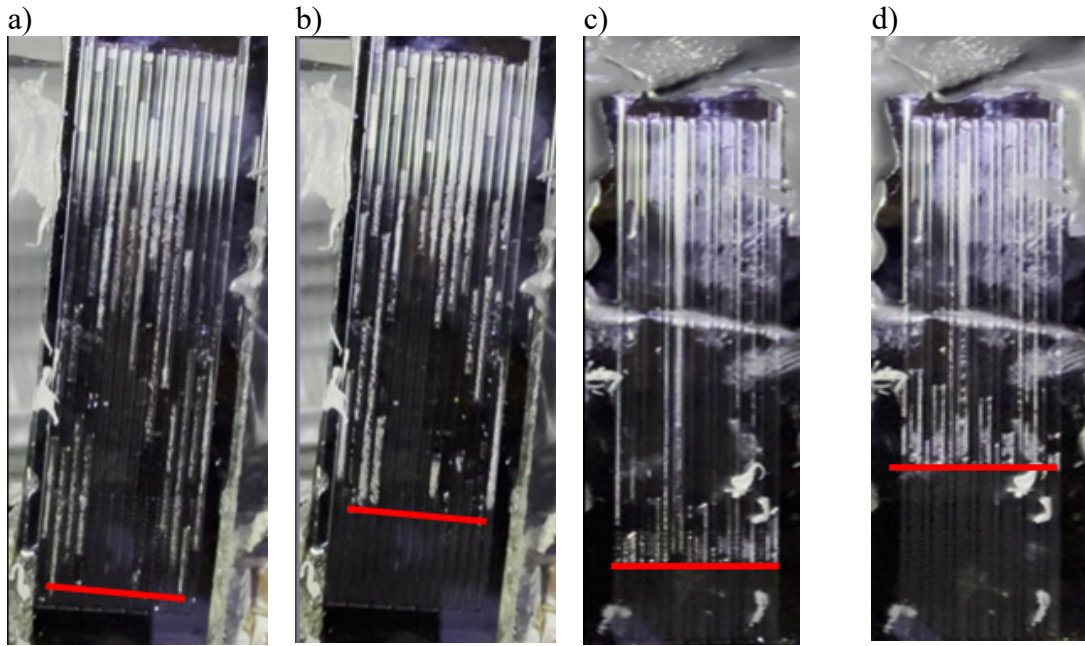


Figure 19: a) Single diameter wick device at $t = 7$ minutes. b) Single diameter wick device at $t = 14$ minutes. c) Dual diameter wick device at $t = 7$ minutes. d) Dual diameter wick device at $t = 14$ minutes.

Single Diameter Wick vs Dual Diameter Wick Power Efficiency

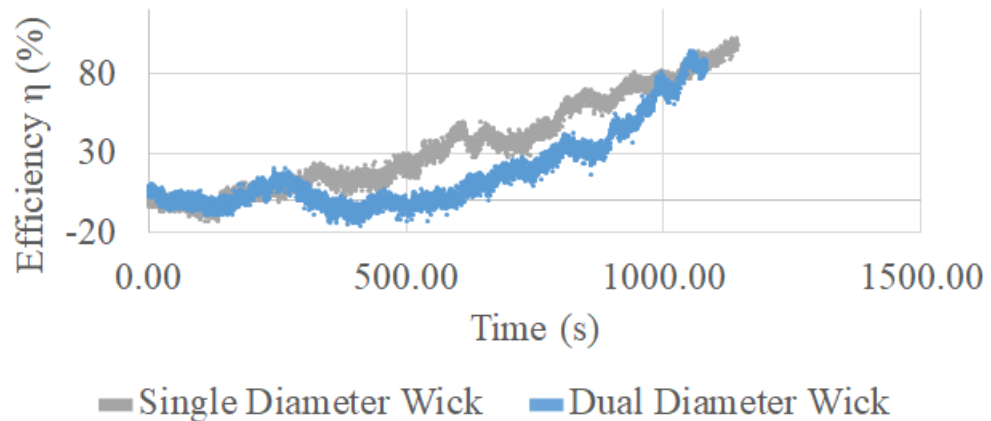


Figure 20: Power efficiency of single diameter and dual diameter wick devices.

In figure 20 above, we examine the power efficiency of both wick structure devices. In spite of the lack of startup, as well as less resistance to dryout, the dual diameter device is able to reach the same power efficiency that the single diameter device does by the end of the experiment. There are two potential explanations. One is that conduction produces a dominant effect. The other is that the device does not experience flow boiling, but rather just boiling, and in the short term, that is enough to produce a significant enough effect that the device performance can rival an operational device. It is likely that the real answer is a combination of these two effects; conduction plus boiling allows the dual diameter wick device to temporarily rival the single diameter wick device in power efficiency. In longer duration experiments, we would then expect that any device that can achieve startup would outperform the dual diameter wick device, especially as it reaches full dryout. This is supported by the fact that according to energy efficiency metrics, the dual diameter wick case is only slightly better than conduction; the effects of convection in these devices are only really apparent at full activation. If the water inside the device is still, then it only really serves as a conduction pathway, and the thermal conductivity of water is low (.6 W/m K). There would of course be other modes of heat transfer (namely the phase change), and these together can still dissipate heat, but without significant motion in the device, it is inevitable that performance will lag behind operational devices. This also serves to explain the discrepancy in energy efficiency of 23.46% between the two devices.

Next, we compare all of the dual diameter devices. While temperature data for the dual diameter reentrant case fluctuates a great deal, we do see an upward trend in

efficiency. As such, we compare a linear fit of the dual diameter reentrant case to the other cases, as shown below in figure 21 below. It is also important to note that the reentrant case leaked during experimentation.

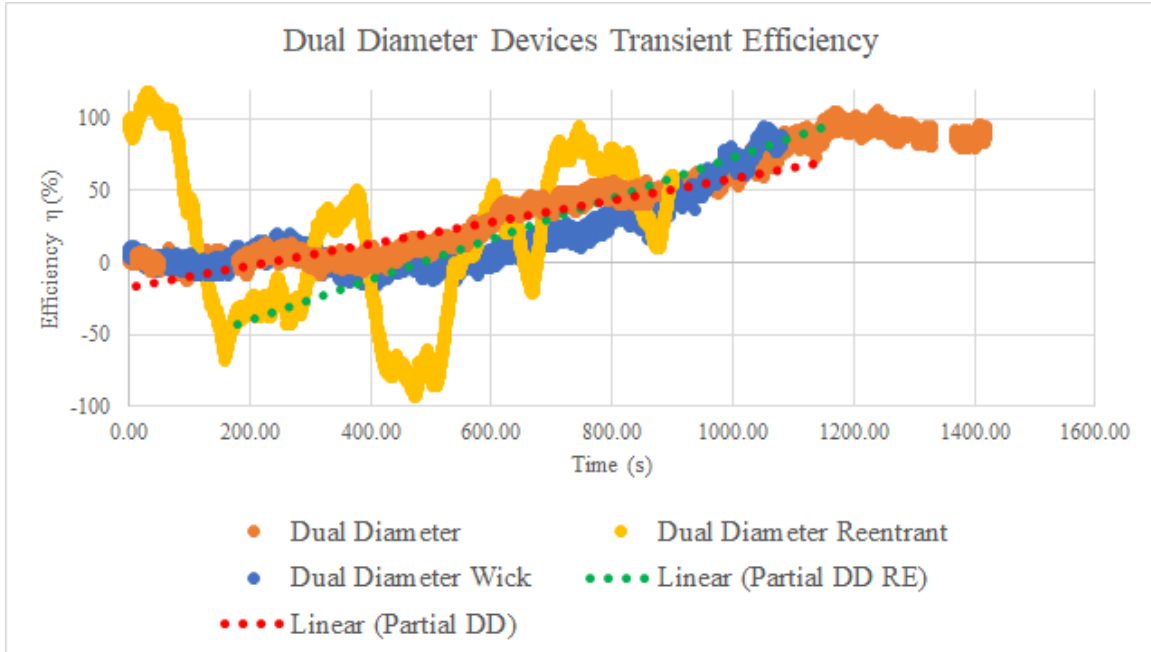


Figure 21: Transient efficiency of all dual diameter devices.

Interestingly, both dual diameter reentrant and dual diameter wick cases seem to initially lag in performance compared to the dual diameter baseline case. In the reentrant case, it seems likely that had it not leaked, its power efficiency would start to beat the baseline case based on the data trend. However, the fact that it leaked severely limited its energy efficiency; a significant portion of the heat that would have been dissipated by the water loop would have instead been dissipated by the environment. This then explains worse energy efficiency than the conduction case (29.32% for the reentrant device compared to 36.92% for the unfilled device). The dual diameter wick case also seems to start to trend

beyond the dual diameter baseline. Again, we believe this is temporary due to the effects of conduction plus boiling, and this is supported by the fact that the overall efficiency is not significantly higher than conduction.

Lastly, while we do not have temperature data for the single diameter reentrant case, we do have video, shown in supplementary information 1. As such, we offer a qualitative analysis of the performance of reentrant structures. From video data, we see that bursts of oscillation seem to be more sustained in reentrant structure devices up until they leak. We also do not believe it is coincidental that both reentrant devices leaked. Leaks may have been caused by more aggressive bubble nucleation. Because the reentrant structures are meant to function as built in nucleation sites, it seems likely that under excessive superheats, a plethora of bubbles would have formed. And our temperatures were certainly excessive for devices filled with water, as shown in figure 14(b). With more bubble generation, internal pressure in these devices would have become significantly higher than baseline cases. Of course, our wick structure devices did not leak, and they also had reentrant structures, but this can be explained through two ways. One is that our wick structure cases were sealed better than our reentrant structures as we had to coat them in several layers of epoxy to prevent diffusion through the PDMS we used to fabricate them before filling them. The other possible explanation is that the wick structures may have had an additional effect of distributing cooled liquid throughout the device, serving to lower pressure throughout the devices without necessarily stopping operation of the devices.

Taken together, the results highlight several key behaviors and unexpected interactions between device geometry, internal structure, and phase change dynamics. While the experimental dataset is limited to a single round of trials due to fabrication delays and equipment constraints, the data collected offers meaningful insight into how startup, oscillation behavior, and dryout resistance are influenced by structural design. The analysis also reveals important trade-offs: dual diameter devices promote startup in baseline cases but may inhibit it when paired with wick structures, while reentrant features appear to enhance nucleation but may also increase the risk of failure under pressure. These findings point to both promising design directions and areas requiring further refinement. The following section discusses these implications in more detail and outlines potential improvements and future work that could expand on the insights presented here.

7. Conclusions & Continuing Work

There are several things that must continue to be refined and developed. First is device filling. The devices that we tested experimentally were all filled under the third filling setup. However, the third filling setup, while capable of generating filled devices, does not do so while keeping devices at particularly low pressures. This in turn impacted the operation of our devices. As such, a shift should be made from the third filling setup to the fourth filling setup, which requires all new fabrication. Additionally, the sealing of these devices presents some issues. While sealing with melted plastic tubing and epoxy can work, we have had some devices leak during experimentation, likely due to

increasing pressures caused by high temperatures inside the devices as well as differing rates of thermal expansion between the epoxy and the devices. As such, a more robust seal will likely be required. There may be more potential with thicker glass capillary tubes, though melting thicker glass to create a seal is not so trivial and may be somewhat dangerous. One potential workaround is to simply fabricate glass covers on devices to be larger than the silicon chips, and instead of through holes for reservoirs, have channels that extend out to the edge of the device. Filling can then be done from the side of the device, and once it is done, melting the glass overhang may be an effective way to seal the devices. This would need to be tested in subsequent rounds of fabrication.

Experimentation on this project is still in its infancy and there is a great deal of work to be done. For example, all of the above results were obtained for a constant heat flux at the evaporator, and a constant temperature at the condenser. Realistically, a CPU is kept at approximately 70 to 100 °C and unless it is overclocked, or CPU heavy applications are used, will stay within that temperature range. However, because we only tested a constant heat flux in which we saw temperatures ranging from 20 to 250 °C, this is not representative of a real electronic system. As such, the following experiments should be done:

1. Sweeps of different high heat fluxes to understand if wick structures improve dryout mitigation.
2. Isothermal experiments in which temperatures are kept roughly constant (roughly because we can only exert control over heat flux via the power supply). Temperatures should be tested ranging from 100 to 200 °C in 25

°C increments. Starting at 100 °C is due to the fact that these devices require some wall superheat for bubble nucleation and because our working fluid is deionized water, these devices should not be able to activate at temperatures below the boiling point of water.

3. Variable load experiments in which temperatures are manipulated in a range of 30 to 50 °C over a longer duration to mimic what may occur in real electronics usage. Temperatures would be changed via heat flux manipulation through the power supply.
4. Variable filling ratios in which each design is tested at filling ratios ranging from 40 to 60% in 5 or 10% increments. Filling ratios can greatly skew the performance of these devices and as such, testing multiple filling ratios would be ideal.
5. Different dielectric fluids such as ethanol and chemically engineered fluids should be tested as fluid properties can have a significant effect on both operating temperature range and performance for these devices. Ethanol is often used in relevant literature to help quantify device performance in a fluid with drastically different properties compared to the properties of water. In a real application, chemically engineered dielectric fluids would be used, and so it is desirable to progress to using these.

In conclusion, while the current work represents a foundational step in both this project and the development of micro oscillating heat pipes, it also highlights the

numerous experimental and engineering challenges that must be addressed both before these devices can be appropriately tested and realistically applied to electronic cooling. Improvements in filling accuracy and sealing reliability are necessary to ensure consistent operation. Furthermore, a systematic experimental framework incorporating realistic thermal loads, varied fluid properties, and optimized filling ratios is essential for generating meaningful performance data. Continued refinement of both the experimental methodology and device design will be critical to advancing these systems toward practical and robust thermal management solutions.

Bibliography

1. Zhang, P., Yuan, P., Jiang, X., Zhai, S., Zeng, J., Xian, Y., Qin, H., & Yang, D. (2017). A theoretical review on Interfacial Thermal Transport at the nanoscale. *Small*, 14(2). <https://doi.org/10.1002/smll.201702769>
2. Pop, E., Sinha, S., & Goodson, K. E. (2006). Heat generation and transport in nanometer-scale transistors. *Proceedings of the IEEE*, 94(8), 1587–1601. <https://doi.org/10.1109/jproc.2006.879794>
3. Akachi, H. (1990, May 15). Structure of a heat pipe. U.S. Patent US4921041A. <https://patents.google.com/patent/US4921041A/en>
4. Akachi, H. (1993, June 15). Structure of a micro-heat pipe. U.S. Patent US5219020A. <https://patents.google.com/patent/US5219020A/en>
5. Wen, J. (2021). Thermal resistance modeling of oscillating heat pipes filled with acetone by using artificial neural network. *Journal of Thermal Analysis and Calorimetry*, 144(5), 1873–1881. <https://doi.org/10.1007/s10973-020-10536-x>
6. Ma, H. (2015). *Oscillating heat pipes*. Springer, New York. <https://doi.org/10.1007/978-1-4939-2504-9>
7. Pouryoussefi, S. M., & Zhang, Y. (2017). Analysis of chaotic flow in a 2D multi-turn closed-loop pulsating heat pipe. *Applied Thermal Engineering*, 126, 1069–1076. <https://doi.org/10.1016/j.applthermaleng.2017.01.097>
8. Thompson, S. M., Ma, H. B., & Wilson, C. (2011). Investigation of a flat-plate oscillating heat pipe with Tesla-type check valves. *Experimental Thermal and Fluid Science*, 35(7), 1265–1273. <https://doi.org/10.1016/j.expthermflusci.2011.04.014>
9. Yuan, D., Qu, W., & Ma, T. (2010). Flow and heat transfer of liquid plug and neighboring vapor slugs in a pulsating heat pipe. *International Journal of Heat and Mass Transfer*, 53(7–8), 1260–1268. <https://doi.org/10.1016/j.ijheatmasstransfer.2009.12.042>
10. Ling, Y., Li, X., Zhang, X., Liu, Z., & Zhao, P. (2023). Experimental and theoretical study on Operation Characteristics of an oscillating heat pipe. *Applied Sciences*, 13(14), 8479. <https://doi.org/10.3390/app13148479>
11. Fang, S., Zhou, C., Zhu, Y., Qian, Z., & Wang, C. (2024). Review on research progress of pulsating heat pipes. *Inventions*, 9(4), 86. <https://doi.org/10.3390/inventions9040086>

12. Wang, P., Xu, D., Jia, P., Shi, Y., Guo, R., & Li, L. (2025). *Effects of Operating and Assembly Parameters on the Horizontal Startup Characteristics of Nitrogen Pulsating Heat Pipes*. Available at SSRN: <https://doi.org/10.2139/ssrn.5184192>
13. Zhang, Q., Tan, S.-C., Zhu, J.-M., Jiang, Y.-Y., & Guo, C. (2025). Heat transfer characteristics of a flat plate pulsating heat pipe with microstructures for unidirectional thermal-to-mechanical energy conversion. *Applied Physics Letters*, 126(5). <https://doi.org/10.1063/5.0250086>
14. Carey, V. P. (2018). *Liquid-Vapor Phase-Change Phenomena*. (2nd ed.). CRC Press, Boca Raton, FL. <https://doi.org/10.1201/9780203748756>
15. Kim, W., & Kim, S. J. (2018). Effect of reentrant cavities on the thermal performance of a pulsating heat pipe. *Applied Thermal Engineering*, 133, 61–69. <https://doi.org/10.1016/j.applthermaleng.2018.01.027>
16. Li, W., Wang, Z., Yang, F., Alam, T., Jiang, M., Qu, X., Kong, F., Khan, A. S., Liu, M., Alwazzan, M., Tong, Y., & Li, C. (2019). Supercapillary architecture-activated two-phase boundary layer structures for highly stable and efficient flow boiling heat transfer. *Advanced Materials*, 32(2). <https://doi.org/10.1002/adma.201905117>
17. Yang, K.-S., Cheng, Y.-C., Liu, M.-C., & Shyu, J.-C. (2015). Micro pulsating heat pipes with alternate microchannel widths. *Applied Thermal Engineering*, 83, 131–138. <https://doi.org/10.1016/j.applthermaleng.2015.03.020>
18. Tseng, C.-Y., Yang, K.-S., Chien, K.-H., Jeng, M.-S., & Wang, C.-C. (2014). Investigation of the performance of pulsating heat pipe subject to uniform/alternating tube diameters. *Experimental Thermal and Fluid Science*, 54, 85–92. <https://doi.org/10.1016/j.expthermflusci.2014.01.019>
19. Weibel, J. A., & Garimella, S. V. (2012). Visualization of vapor formation regimes during capillary-fed boiling in sintered-powder heat pipe wicks. *International Journal of Heat and Mass Transfer*, 55(13–14), 3498–3510. <https://doi.org/10.1016/j.ijheatmasstransfer.2012.03.021>
20. Diao, Y. H., Liu, Y., Zhao, Y. H., & Wang, S. (2014). Evaporation/boiling heat transfer performance in a sintered copper mesh structure. *Journal of Heat Transfer*, 136(8). <https://doi.org/10.1115/1.4027349>
21. Xie, Q., Xin, F., Park, H. G., & Duan, C. (2016). Ion transport in graphene nanofluidic channels. *Nanoscale*, 8(47), 19527–19535. <https://doi.org/10.1039/c6nr06977k>

22. Satyanarayana, S., Karnik, R. N., & Majumdar, A. (2005). Stamp-and-stick room-temperature bonding technique for microdevices. *Journal of Microelectromechanical Systems*, 14(2), 392–399. <https://doi.org/10.1109/jmems.2004.839334>

VITA

Michael Shohet was born in Boston, MA. He earned his Bachelor of Arts degrees in Economics and Legal Studies from the University of Massachusetts Amherst in May 2020, graduating cum laude. After working in various roles that combined problem solving with business and legal considerations, he pursued a Master of Science in Mechanical Engineering at Boston University through the LEAP program, concentrating in Microelectromechanical systems (MEMS) and Nanotechnology. His master's research focuses on micro-scale oscillating heat pipes for enhanced electronic cooling and was done through the NEFT lab under Professor Chuanhua Duan.

Following the completion of his degree, Michael plans to pursue a career in Mechanical Engineering with a focus on Computational Fluid Dynamics (CFD). He can be reached through email at mis75@bu.edu.

ProQuest Number: 31999823

INFORMATION TO ALL USERS

The quality and completeness of this reproduction is dependent on the quality
and completeness of the copy made available to ProQuest.



Distributed by

ProQuest LLC a part of Clarivate (2025).

Copyright of the Dissertation is held by the Author unless otherwise noted.

This work is protected against unauthorized copying under Title 17,
United States Code and other applicable copyright laws.

This work may be used in accordance with the terms of the Creative Commons license
or other rights statement, as indicated in the copyright statement or in the metadata
associated with this work. Unless otherwise specified in the copyright statement
or the metadata, all rights are reserved by the copyright holder.

ProQuest LLC
789 East Eisenhower Parkway
Ann Arbor, MI 48108 USA